J. Fluid Mech. (1984), *vol.* 144, *pp.* 13–46
Printed in Great Britain

Unsteady measurements in a separated and reattaching flow

By N. J. CHERRY†, R. HILLIER AND M. E. M. P. LATOUR
Department of Aeronautics, Imperial College, London

(Received 6 March 1983 and in revised form 20 February 1984)

Measurements of fluctuating pressure and velocity, together with instantaneous smoke-flow visualizations, are presented in order to reveal the unsteady structure of a separated and reattaching flow. It is shown that throughout the separation bubble a low-frequency motion can be detected which appears to be similar to that found in other studies of separation. This effect is most significant close to separation, where it leads to a weak flapping of the shear layer. Lateral correlation scales of this low-frequency motion are less than the reattachment length, however; it appears that its timescale is about equal to the characteristic timescale for the shear layer and bubble to change between various shedding phases. These phases were defined by the following observations: shedding of pseudoperiodic trains of vortical structures from the reattachment zone, with a characteristic spacing between structures of typically 60 % to 80 % of the bubble length; a large-scale but irregular shedding of vorticity; and a relatively quiescent phase with the absence of any large-scale shedding structures and a significant 'necking' of the shear layer downstream of reattachment.

Spanwise correlations of velocity in the shear layer show on average an almost linear growth of spanwise scale up to reattachment. It appears that the shear layer reaches a fully three-dimensional state soon after separation. The reattachment process does not itself appear to impose an immediate extra three-dimensionalizing effect upon the large-scale structures.

1. Introduction

Despite many experimental studies of separated-and-reattaching flows there is still relatively little known about the unsteady flow structure generated by even the simplest of geometries. This largely results from difficulties with instrumentation, since conventional hot-wire anemometry is not possible in regions of high turbulence intensity or instantaneous flow reversal. In turn, measurements using pulsed-wire (e.g. Moss & Baker 1980) or laser anemometry (e.g. Etheridge & Kemp 1978), or surface probes for instantaneous skin friction or flow direction (e.g. Westphal, Eaton & Johnston 1980; Castro & Dianat 1983) are still scarce and are also subject to their own difficulties of operation or interpretation. A knowledge of the unsteady processes is essential however, both in order to improve our physical understanding of the controlling phenomena, and also to provide comparative data against which the various calculation methods now under development can be tested.

The present study investigates the unsteady separated and reattaching flow formed by the two-dimensional rectangular leading-edge geometry shown in figure 1. This geometry was selected because of two important simplifying features: the geometrically fixed separation positions, and the highly favourable pressure gradient

† Present address: Central Electricity Research Laboratories, Leatherhead, Surrey.

on the front face which means that the separating shear layer is extremely thin compared with the overall bubble scale.

Other experiments on this or related configurations to investigate the unsteady structure of the flow field are very rare, although some general features common to two-dimensional separations are now becoming established. First, instantaneous flow visualizations or the use of special surface-mounted pulsed-wire anemometers (e.g. Westphal *et al.* 1981; Gartshore & Savill 1982), and also time-dependent calculations such as the discrete-vortex method (e.g. Ashurst 1979; Kiya, Sasaki & Arie 1982) all show that shear-layer reattachment is a highly unsteady process. Gartshore & Savill (1982), for example, have reported the irregular formation of large structures downstream of reattachment for a normal flat-plate/splitter-plate combination, and have suggested that the 'instantaneous reattachment' position moves over a distance of up to 50% of the time-averaged reattachment length. A similar observation was made by Eaton & Johnston (1981) for the flow over a rearward-facing step.

This irregular and sometimes large-scale shedding of vorticity from the reattachment zone causes the maximum shear-layer Reynolds stresses and surface-pressure fluctuations to occur in the vicinity of reattachment. In a study of a variety of two-dimensional separated-and-reattaching flows Mabey (1971) used pressure-fluctuation data to show that the characteristic reduced shedding frequency was correlated well between different configurations when normalized by the reattachment length. He suggested that this showed a feedback mechanism, whereby the shedding of vorticity from reattachment interacted with the formation of disturbances near separation, although details of this interaction are not clear.

For regions upstream of reattachment various workers have compared the development of the separated shear layer with plane mixing layers. McGuinness (1978), for example, has made a very detailed study of the internal separated flow at the inlet to a parallel pipe. He showed that for the first 75% or so of the bubble length the shear-layer development was very close to that of a mixing layer, in terms of growth rate, development of coherent structures and characteristic frequencies. It appears that only at a relatively late stage does the presence of the reattachment surface disrupt this similarity.

There are very few measurements of the spanwise correlation scales for the unsteady development of the shear layer, although these are crucial to any numerical of physical modelling of the flow. Most relevant data have been obtained for the plane mixing layer, that is, in the absence of a reattachment surface. Preliminary measurements by Hillier & Cherry (1981*a*) on the present geometry, and also data of Katsura (1976) for a similar geometry, suggest that spanwise correlation scales for surface-pressure fluctuations at reattachment are of the order of 30% of the reattachment length. In fact these are comparable to those expected for plane mixing layers.

One feature which has characterized several studies of separated-and-reattaching flows is a low-frequency unsteadiness at timescales large compared with the particle transit time between separation and reattachment. This is present in data of Fricke (1971) for pressure fluctuations immediately downstream of a surface-mounted fence, although he does not comment on it. It has also been reported by Eaton & Johnston (1981) for a rearward-facing step, by McGuinness (1978) for a separation in the inlet region of a pipe, and by Hillier & Cherry (1981*a*) and Kiya *et al.* (1982) for the present configuration. No satisfactory explanation for this phenomenon has yet appeared in the literature, and it is therefore given very careful consideration in this paper.

The data presented and discussed here extend the preliminary investigations of

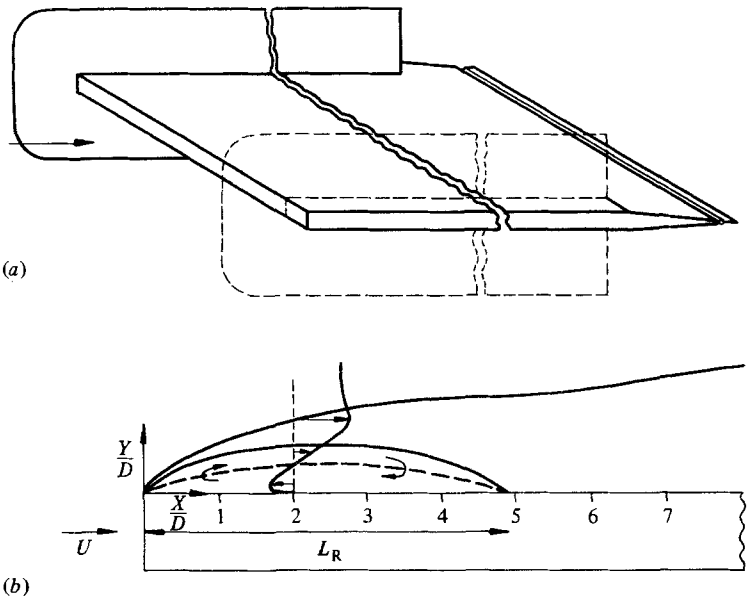

FIGURE 1. (*a*) Model tested. (*b*) Schematic of mean-flow field. X, Y and Z respectively are measured in the direction of the freestream, normal to the model surface and in the spanwise direction. Model thickness $D = 38.1$ mm.

Hillier & Cherry (1981*a*) and Kiya *et al.* (1982) by adding: spectral measurements of velocity and surface-pressure fluctuations; space–time correlations for pressure–pressure, velocity–velocity and pressure–velocity combinations; and correlations of instantaneous smoke-flow visualizations of the separated region with corresponding surface-pressure time histories. Since hot-wire errors are large in regions of high turbulence intensity, velocity measurements are confined to the low-intensity and unsteady irrotational regions outside the shear layer. Nevertheless, particularly when correlated with surface-pressure fluctuations, much can be deduced from these velocity measurements concerning the larger-scale shear-layer motions.

2. Experimental equipment and procedure

The two-dimensional test model is shown in figure 1. This had a thickness D of 38.1 mm and a total chord of 1.37 m. The trailing edge was streamlined to minimize any wake-induced unsteadiness. The model spanned the 0.6 m width of a 0.6 m × 1.0 m test section closed-circuit wind tunnel, giving a solid blockage of 3.79 %. The endplates shown in figure 1 were always employed, usually at an aspect ratio (span between end plates/D) of 13.2, since Brederode (1975) has shown that their use is essential. The model was placed at zero incidence to the nominally smooth stream (approximately 0.07 % turbulence intensity), and a trailing-edge flap was used to remove any residual flow asymmetry top-to-bottom. Agreement was always within 0.01 in C_p between equivalent positions on the upper and lower surfaces. The test Reynolds number Re_D, based upon the model thickness and the approaching freestream velocity, was held in the range $3.2 \times 10^4 \pm 0.2 \times 10^4$.

Fluctuating pressures were measured with Setra 237 low-pressure transducers mounted within the model. These were fitted with caps and connected by short lengths of tubing to tappings of 1.66 mm internal diameter and 2 cm length. This

Acoustic mode/comments	Frequency n (Hz)	$\frac{nD}{U_\infty}$	$\frac{nL_R}{U_\infty}$
Blade-passing frequency of fan	29	0.103	0.504
Twice blade-passing frequency	58	0.206	1.01
Longitudinal standing wave	22	0.078	0.382
Other	80	0.285	1.39

TABLE 1. Principal acoustic modes at the test speed

system was dynamically calibrated against a flush-mounted microphone, and showed the onset of a Helmholtz resonance above about 700 Hz. Gain variations up to 500 Hz, or $nD/U_\infty = 1.5$, were less than $\pm 10\,\%$, which provided an adequate frequency range for the test speed but prohibited useful measurements at significantly higher Reynolds numbers. Pressure spectra and r.m.s. values have been corrected for this gain change, but no allowance has been made for the resolution due to the finite pressure tapping size. This was calculated to attenuate the signal by some 5 % at 500 Hz and was not therefore important in these measurements, where the majority of the pressure energy was always below 100 Hz. Pressure–pressure and pressure–velocity correlations have not been corrected, either for gain variations or for the slight phase-angle errors of the pressure transducers. The resulting effect on both amplitude, and on the effective spatial shifting due to phase error, are estimated as less than $\pm 5\,\%$ and $0.05D$ respectively.

Cherry (1982) has carried out an extensive acoustic calibration of the empty tunnel. This showed only weak r.m.s. pressure fluctuations at the test speed (acoustic r.m.s. pressure coefficient less than 0.52 %), the principal modes being listed in table 1. Comparison of these acoustic data with spectral measurements of surface pressure in the separated-flow region (§7), shows that acoustics are relatively very weak and that there is no evidence that they excite any corresponding narrow-band shear-layer fluctuations.

The instantaneous smoke-flow visualizations of §6 were obtained by introducing smoke from a narrow slot 30 mm long in the spanwise direction on the front face near the separation edge. Perspex endplates were used for these visualizations, which were conducted at the same speed as the remainder of the measurements so that they can be considered truly representative. This injection system provided sufficient density of smoke for visualizations to be made well downstream of reattachment, although as a consequence it becomes difficult to discern details of the interior flow in the cavity. Instead, the visualizations reveal more clearly the intermittent edge of the shear layer, and hence the larger-scale structures which are of interest here. The flow was illuminated by a white-light strobe flash of about 30 μs duration, focused by a cylindrical lens system to give a sheet of light some 8 mm in width on the model centreline.

3. Transition, aspect ratio and blockage effects

At the test Reynolds number, separation of the front-face boundary layer is laminar, with an estimated momentum thickness θ_{sep} of about $0.004D$. Smoke flow visualizations presented earlier (Hillier & Cherry 1981*a*) showed that shear-layer transition was completed within about $0.3D$ of separation, the first visible disturbances

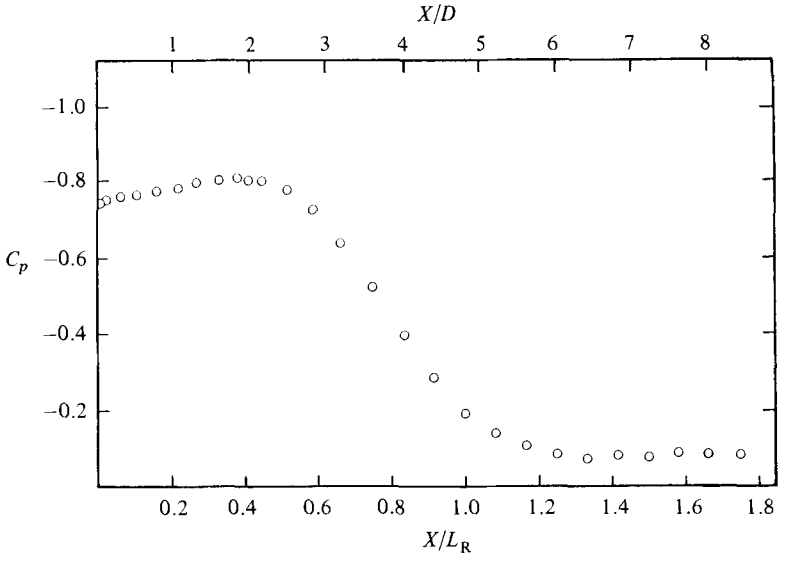

FIGURE 2. Mean-pressure distribution uncorrected for blockage.

occurring within half this distance. This compares with a centreline reattachment length L_R (measured from surface oil flows) of $4.9D \pm 0.05D$. Both the reattachment length and the mean-pressure distribution of figure 2 were unchanged for Reynolds-number increases up to 6×10^4. A weak progressive elongation of the bubble appeared when the Reynolds number was reduced below 3×10^4. This corresponded to the gradual extension of the laminar shear layer seen in the visualizations of Hillier & Cherry. Figures 3(*a*, *b*) show instantaneous smoke-flow visualizations at a Reynolds number Re_D of only 5×10^3. In each case the first laminar disturbance is visible at about $X/D \approx 0.2$, with turbulent structures evident from $X/D = 0.75$ onwards. These visualizations also illustrate the vortex growth/coalescence process found in many mixing-layer experiments. Although the Reynolds number of the main tests is significantly higher than this, a similar growth process can be seen later in some of the visualizations presented in §6.

It is worth making a brief comment here on the effects of blockage and aspect-ratio variations upon the reattachment length, since these aid comparison with other experiments on nominally similar flows. The aspect ratio of 13.2 was the highest achievable with endplates, and was about six times the spanwise correlation scale (see §9) and 2.7 times the reattachment length L_R. At this aspect ratio the reattachment line was found to curve slightly across the span, so that the mean flow field is not free from three-dimensional effects. Nonetheless, the dependence of L_R on aspect ratio is weak, as shown in figure 4, which also includes other data taken in the same wind tunnel with similar geometries at different blockages, by Latour & Hillier (1980) and by Brederode (1975). Each of these three sets of data appears to asymptote at the highest aspect ratio to a value dependent upon blockage. For the present geometry this is taken as $4.9D \pm 0.05D$. The variation of this asymptotic value with blockage is shown in figure 5, which also includes high-aspect-ratio data from Cheung (1982) and Roshko & Lau (1965). A data point is also included from Kiya *et al.* (1982), and although their tests were conducted at effectively zero blockage, their measurements are low compared with the trend of the remainder of

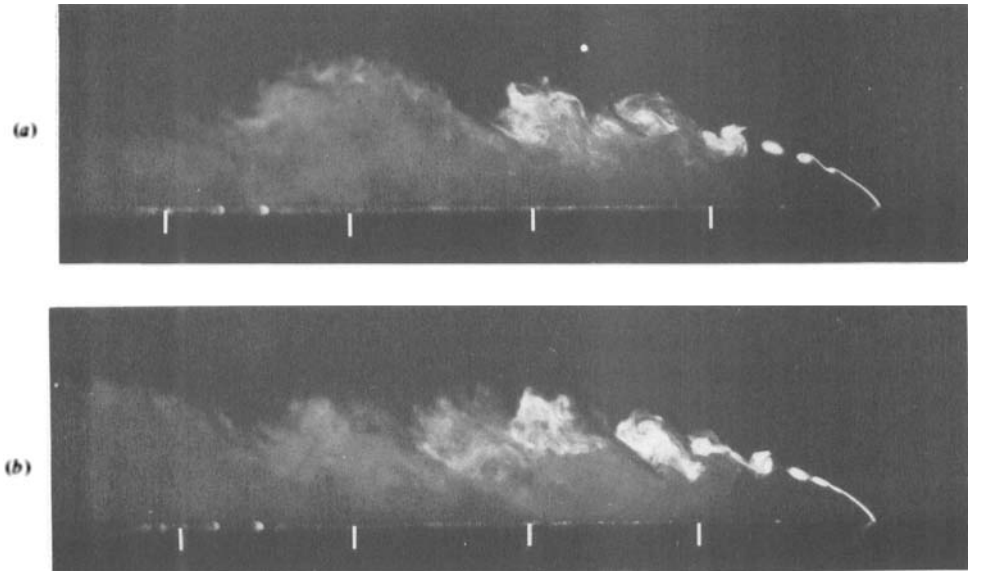

FIGURE 3. Instantaneous smoke flow visualization for $Re_D \approx 5 \times 10^3$. Flow from right to left. Streamwise increments in X of D are marked.

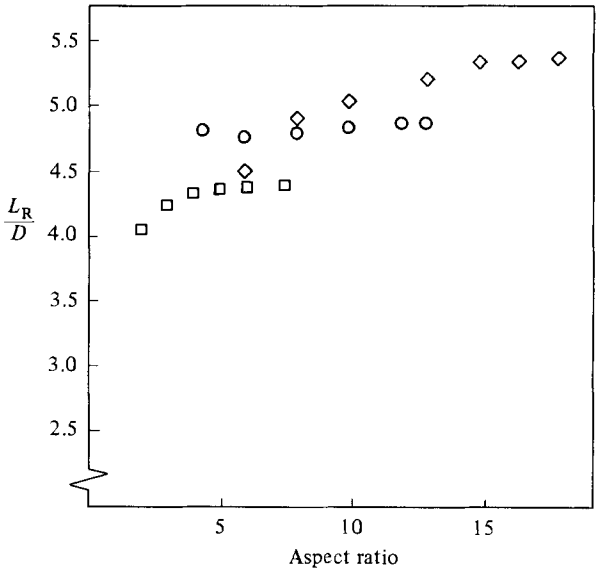

FIGURE 4. Dependence of centreline reattachment length L_R on aspect ratio: ○, present tests; ◇, Latour & Hillier (1980) for 2% blockage; □, Brederode (1975) for 5% blockage.

the data. This may reflect the slight differences in the background-stream turbulence levels (0.3% for Kiya *et al.* and 0.07% during the present experiments), since it is known that the reattachment length is very sensitive to stream turbulence (Hillier & Cherry 1981*b*; Cherry 1982). However, also of significance is that Kiya *et al.* made their measurements without endplates at an aspect ratio of only 10.

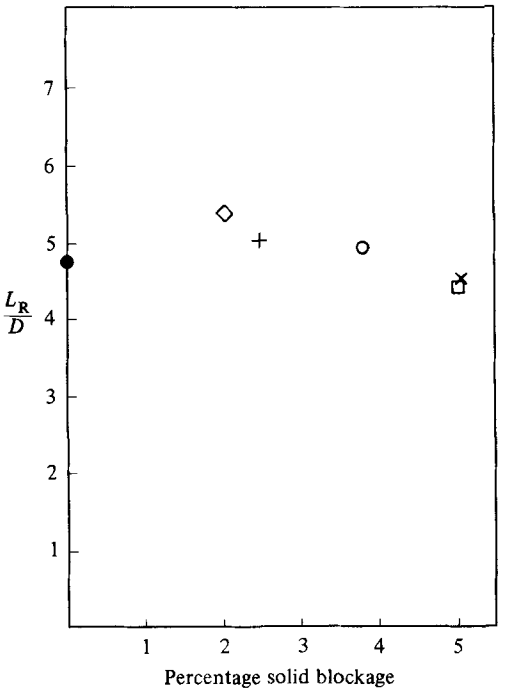

FIGURE 5. Dependence of L_R on blockage: ○, present tests; ◇, Latour & Hillier (1980); □, Brederode (1975); ×, Roshko & Lau (1965); +, Cheung (1982); ●, Kiya *et al.* (1982).

4. Measurements of mean and fluctuating velocity

Figures 6 and 7 show the mean and r.m.s. fluctuating velocity profiles at various streamwise stations. Hot-wire measurements become increasingly in error once the local turbulence intensity exceeds 25% or so, and these data are presented mainly to give a qualitative impression of the bubble scale and the shear-layer thickness rather than for any precise quantitative interpretation. In both cases the velocity is normalized by U_{max}, which is the maximum mean velocity measured at each station, and in figure 6 the y-ordinate is normalized by the streamwise distance, X, from separation, which reveals the nearly linear growth of the shear layer up to reattachment. This is also illustrated in figure 8, which shows the variation with streamwise distance of a maximum-slope thickness δ_{ms}, defined by

$$\delta_{ms} = \frac{U_{max}}{(dU/dy)_{max}},$$

which departs from the conventional vorticity thickness definition only in that it does not incorporate a mean (reversed) velocity on the low-speed side of the shear layer. This figure also takes account of a slight displacement of the zero origin X_0 and includes data from Ota & Itasaka (1976) and Kiya *et al.* (1982) for the present geometry, Arie & Rouse (1956) for the normal flat-plate–splitter-plate combination, Chandrsuda (1976) for the rearward-facing step (chosen because in this case the boundary-layer thickness at separation is thin), and McGuinness (1978) for a separation in the inlet region of a pipe. Also included are data from the pulsed-wire measurements of Moss & Baker (1980) for the forward- and rearward-facing step flows, and of I. Lunnon (1983 private communication) for the normal flat-plate–splitter-plate combination. Within the expected accuracy of hot-wire measurements

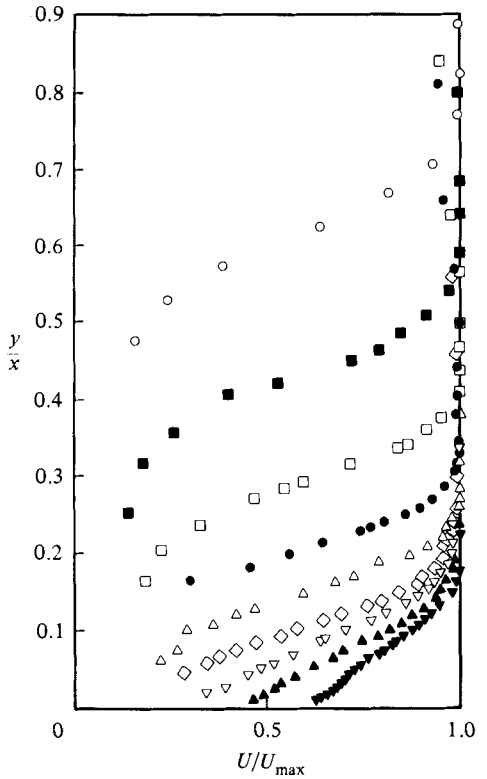

FIGURE 6

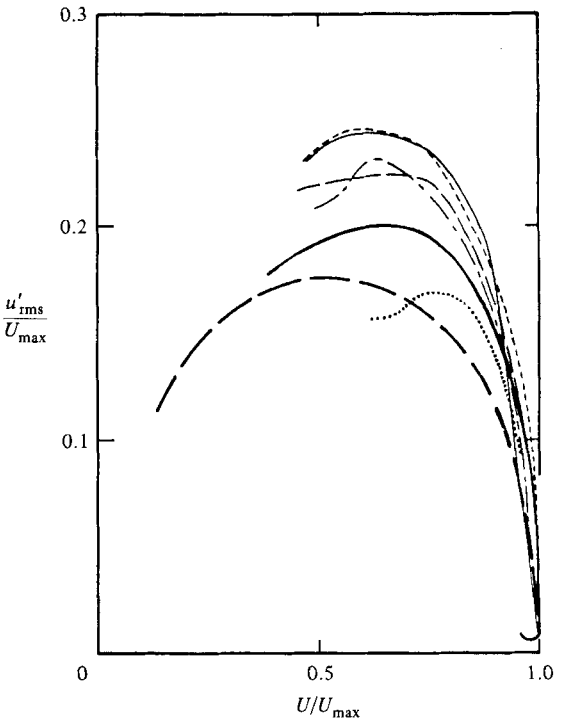

FIGURE 7

FIGURE 6. Profiles of the time-averaged streamwise velocity measured with a single-sensor hot wire at various stations: ○, $X/L_R = 0.102$; ■, 0.217; □, 0.409; ●, 0.613; △, 0.813; ◇, 1.02; ▽, 1.23; ▲, 1.43; ▼, 1.84.

FIGURE 7. Root-mean-square fluctuating-velocity profiles measured with a single sensor hot-wire anemometer at various streamwise stations: ——, $X/L_R = 0.102$; — —, 0.613; – – –, 0.813; ——, 1.02; —·—, 1.23; ·····, 1.84; ——, single-stream mixing layer (Wygnanski & Fiedler 1970).

there is a good correlation between the various experiments, suggesting that the mean mixing-layer growth rate is not very sensitive to the geometrical configuration. Indeed, the scatter in growth rates, which takes an average value of 0.17 for $\mathrm{d}(\delta_{ms})/\mathrm{d}x$ in figure 8, is no worse than that found for the single-stream mixing layer (i.e. with effectively zero velocity on one side). Brown & Roshko (1974), for example, cite for this case values from 0.145 to 0.22 (Wygnanski & Fiedler 1970) for the growth rate of vorticity thickness.

The form of presentation of the intensity profiles in figure 7 enables the profiles to be compared more easily, but still takes no physical account of the time-averaged flow reversal near the surface. The largest values occur in the vicinity of reattachment, which again compares reasonably with other separated flow studies, although levels are distinctly greater than in the plane single mixing layer of Wygnanski & Fiedler (1970) shown for comparison.

5. Preliminary data for fluctuating pressures

Figure 9 presents the variation of the r.m.s. fluctuating pressure coefficient $C_{p'}$ along the model centreline, uncorrected for blockage. These measurements have been discussed by Hillier & Cherry (1981*a*) and are in reasonable agreement with

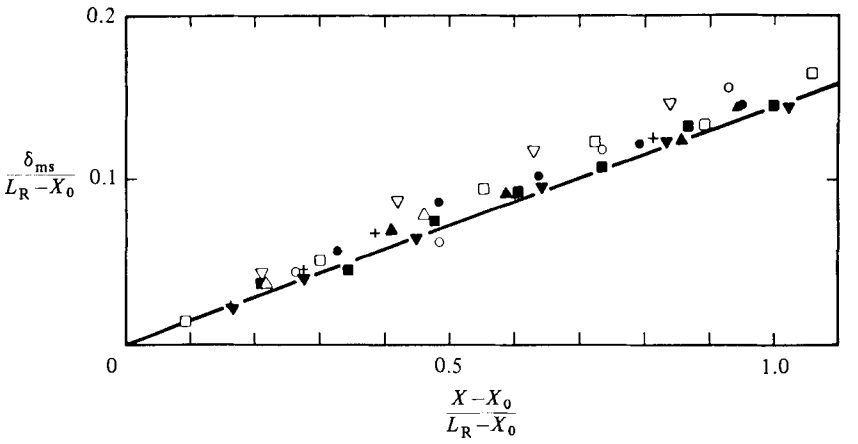

FIGURE 8. Growth of maximum slope thickness for the present measurements and for other geometries taken from the literature: ——▼, present measurements (hot wire); ○, Ota & Itasaka (1976), present geometry (hot wire); ▽, Kiya *et al.* (1982), present geometry (hot wire); □, Chandrsuda (1976), rearward-facing step (hot wire); △, Arie & Rouse (1956), normal flat-plate–splitter-plate (hot wire); +, McGuinness (1978), internal separated flow at pipe entry (hot wire); ●, Moss & Baker (1980), rearward-facing step (pulsed wire); ▲, Moss & Baker (1980) forward-facing step (pulsed wire); ■, Lunnon (1983 private communication), normal flat-plate–splitter-plate (pulsed wire).

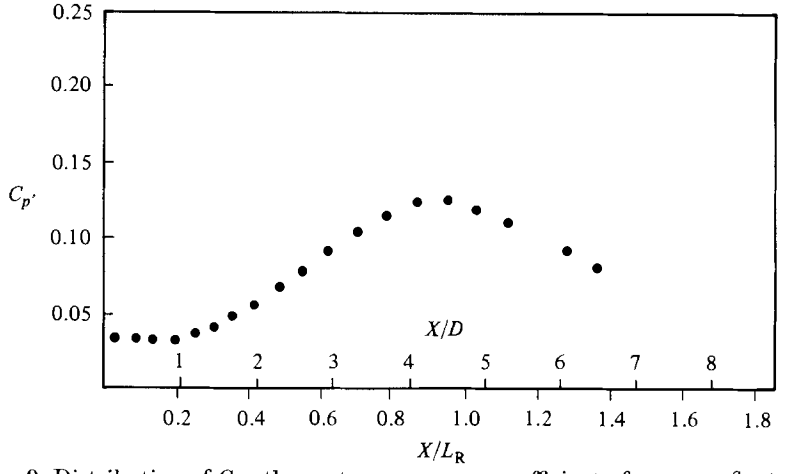

FIGURE 9. Distribution of $C_{p'}$, the root-mean-square coefficient of pressure fluctuation.

measurements on the same geometry by Kiya *et al.* (1982) and Katsura (1976). It is sufficient to remark here that, in common with most two-dimensional studies in non-turbulent streams, the fluctuations increase from a minimum near separation to a maximum slightly upstream of reattachment in a region of strong mean pressure recovery. Various workers have therefore attempted to model reattachment-pressure fluctuations by some form of quasi-steady process driven by large-scale elongations or contractions of the bubble. In fact the evidence of calculations such as the discrete-vortex model of Kiya *et al.* (1982), as well as the flow visualization and correlation measurements of the present work, do not support this view. Rather, it is indicated that the main pressure sources are convective motions with scales less than the reattachment length. Figures 10 and 11, for example, show respectively the streamwise cross-correlation without time lag of surface-pressure fluctuations obtained

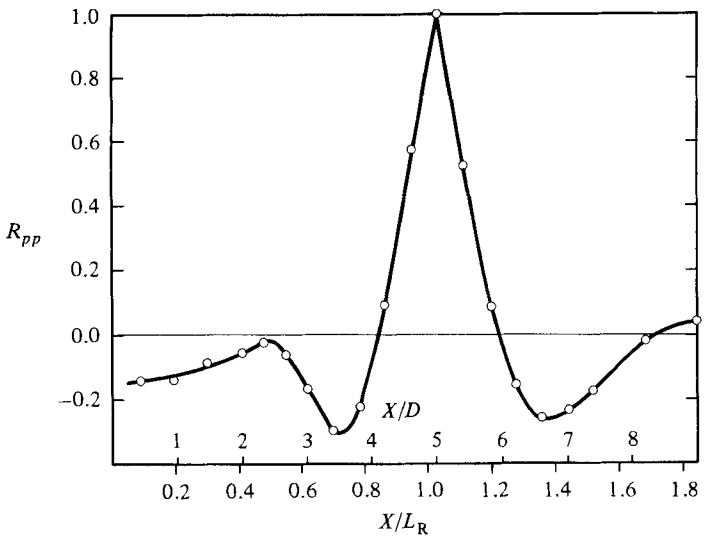

FIGURE 10. Pressure cross-correlation at zero time delay with fixed transducer at $X/D = 5.00$ ($X/L_R = 1.02$).

with a fixed transducer close to the mean reattachment point, and also the time-lagged correlations for specific transducer separations. Figure 11 shows a clear convective motion in the mainstream direction, whilst the spacing between the negative lobes at $X/D = 3.4$ and $X/D = 6.6$ in figure 10 provides a measure of the streamwise scales of these pressure-generating structures at reattachment. The negative correlation between reattachment and separation in figure 10 is probably indicative of a weak quasi-steady process, however, and, as will be seen shortly, the surface-pressure fluctuations near separation are dominated by very-low-frequency motions.

6. Combined smoke flow visualizations and instantaneous-pressure records

All the instantaneous smoke flow visualizations of figures 12–19 were selected from a large number to illustrate typical phases which characterize the unsteady shedding of vorticity from the bubble. Since spanwise correlation scales are only of order $1.5D$–$2.0D$ (see §9), several such phases probably exist simultaneously across the span.

In figures 12 and 13 vorticity is shed from the bubble as a series of more-or-less discrete turbulent structures with characteristic streamwise spacings of order 60–80 % of L_R, which is comparable to the scales found in the earlier correlation measurements of figure 10. Corresponding quasi-periodic bursts of several cycles duration can occur in the surface-pressure signal, as illustrated by figure 13(*b*) where the synchronized pressure trace (measured as a perturbation from the mean value) at $X/L_R = 0.97$ on the model centreline is shown. Here $T = 0$ is the instant of the photograph, and negative and positive times correspond to the pressure histories immediately preceding and following. At $T = 0$ the pressure shows a positive departure from the mean, with the visualization showing that the tapping is located below a shear layer trough, or inroad of irrotational fluid, between the vortical structure which has just been shed from the bubble and the next, forming in the rearmost half of the reattachment zone. Qualitatively this is very similar to the relationship between pressure perturbation and vortex clouds shown by the (two-dimensional) discrete-

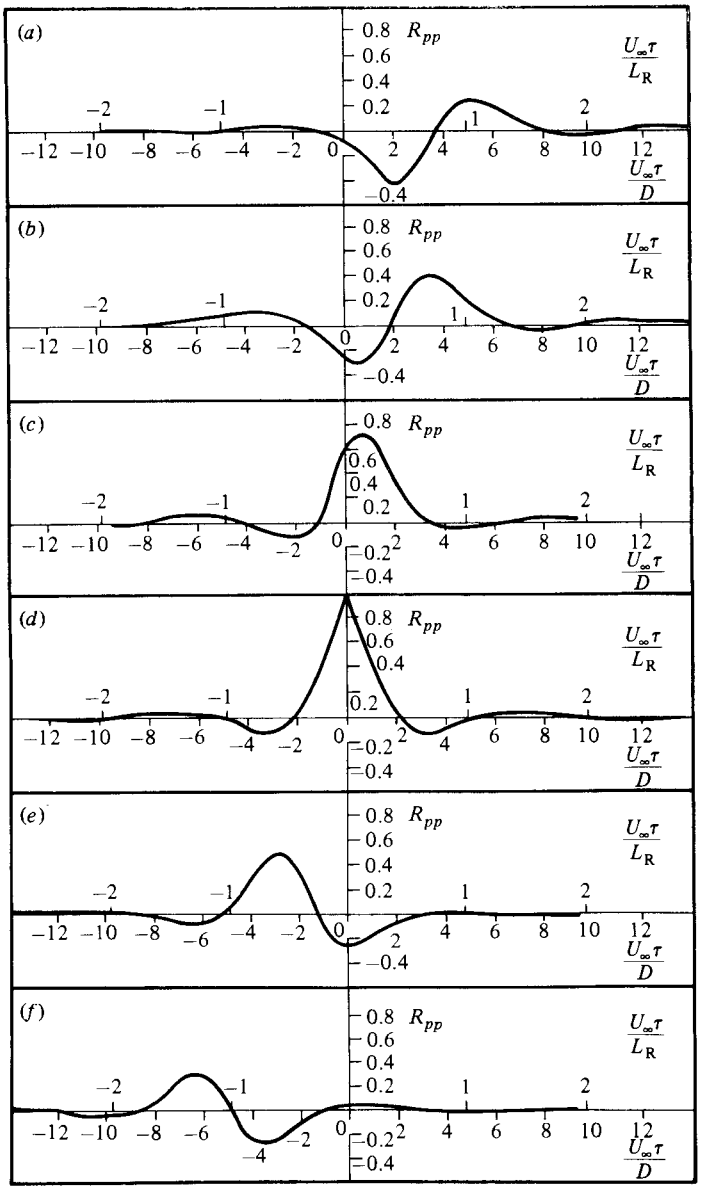

FIGURE 11. Time-lagged pressure cross-correlations with fixed transducer at $X/L_R = 1.02$. Moveable transducer at: (*a*) $X/L_R = 0.547$; (*b*) 0.699; (*c*) 0.945; (*d*) 1.02; (*e*) 1.35; (*f*) 2.03. Positive time delay corresponds to moveable transducer delayed.

vortex computations of Kiya *et al.* (1982) for the same geometry. The suction peaks correspond to the convection of successive vortex cores, or centres of vorticity, over the pressure tapping. Generally the pseudoperiodic pressure signal is highly modulated and appears as a packet of only several cycles duration, as shown in figure 14, where the photograph and pressure traces appear to have been recorded during a period where a regular shedding phase is disappearing. The figure also indicates that substantial variations of pressure are by no means rare.

The pseudoperiodicity shown above similarly appeared in velocity traces when the

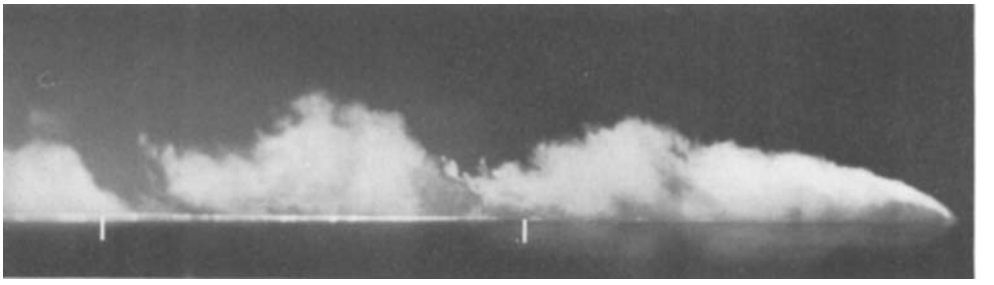

FIGURE 12. Instantaneous smoke flow visualization on model centreline ($Z = 0$). Flow from right to left. Marks indicate $X/L_R = 1.0$ and $X/L_R = 2.0$. $Re_D \approx 3.2 \times 10^4$.

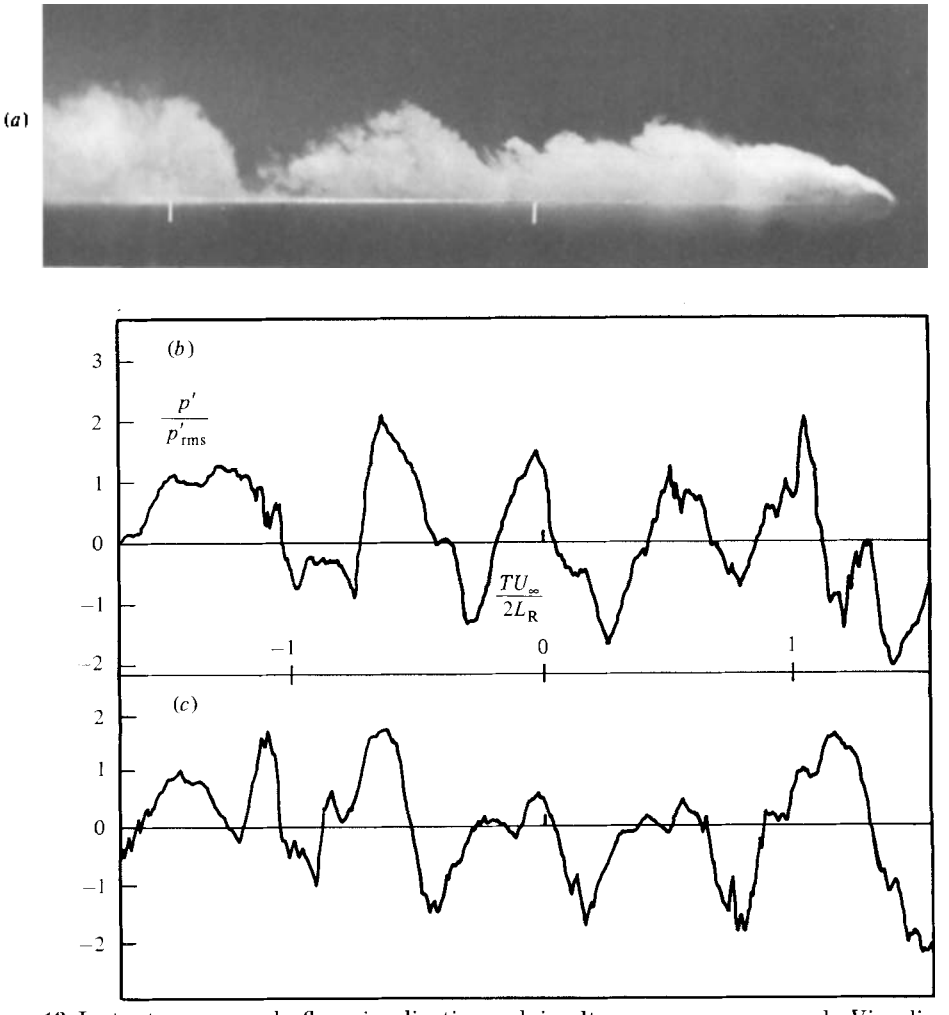

FIGURE 13. Instantaneous smoke flow visualization and simultaneous pressure records. Visualization comments as for figure 12. Pressure trace (*b*) recorded at $X/L_R = 0.97$, $Z = 0$; (*c*) recorded at $X/L_R = 0.97$, $Z/L_R = 0.2$. The pressure is expressed as perturbation from the local mean value normalized by the local r.m.s. value. Timescale normalized by $0.5U_\infty$, which represents quite closely the characteristic disturbance convection speed in the vicinity of reattachment.

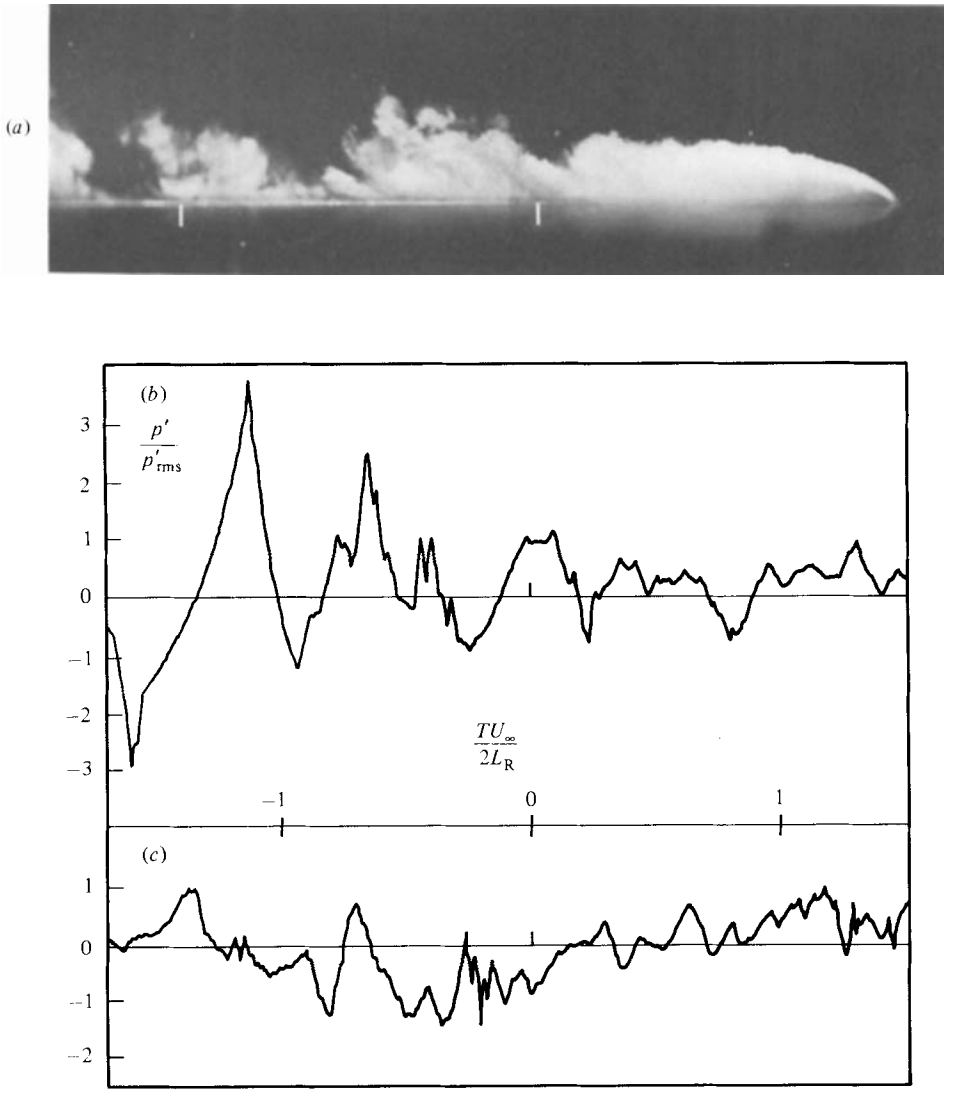

FIGURE 14. Instantaneous smoke flow visualization and simultaneous pressure records. Visualization comments as for figure 12. Pressure trace (*b*) recorded at $X/L_R = 0.97$, $Z = 0$; (*c*) recorded at $X/L_R = 0.27$, $Z = 0$.

hot wire was located at the shear-layer edge in the irrotational or low intermittency region. It was not possible to record hot-wire signals simultaneously with the smoke flow visualizations, but figure 20 shows instead two sequences where pressure and velocity signals were recorded together, the pressure transducer being located on the model centreline at $X/L_R = 0.97$ and the hot wire immediately above it at $Y/D = 1.55$ (where $u'_{\rm rms}/U_\infty = 2.5\,\%$ and the signal is essentially irrotational). The two signals are broadly in antiphase, as expected for pressure and velocity fluctuations on opposite sides of a vortex structure (the long-time-averaged correlation between the two is about -0.65), and typical pseudoperiodic bursts occur in figure 20(*a*), commencing at $TU_\infty/D = 0$, and in figure 20(*b*), at $TU_\infty/D = 46$. It can be seen that extreme pressure fluctuations do not always correspond to extreme velocity

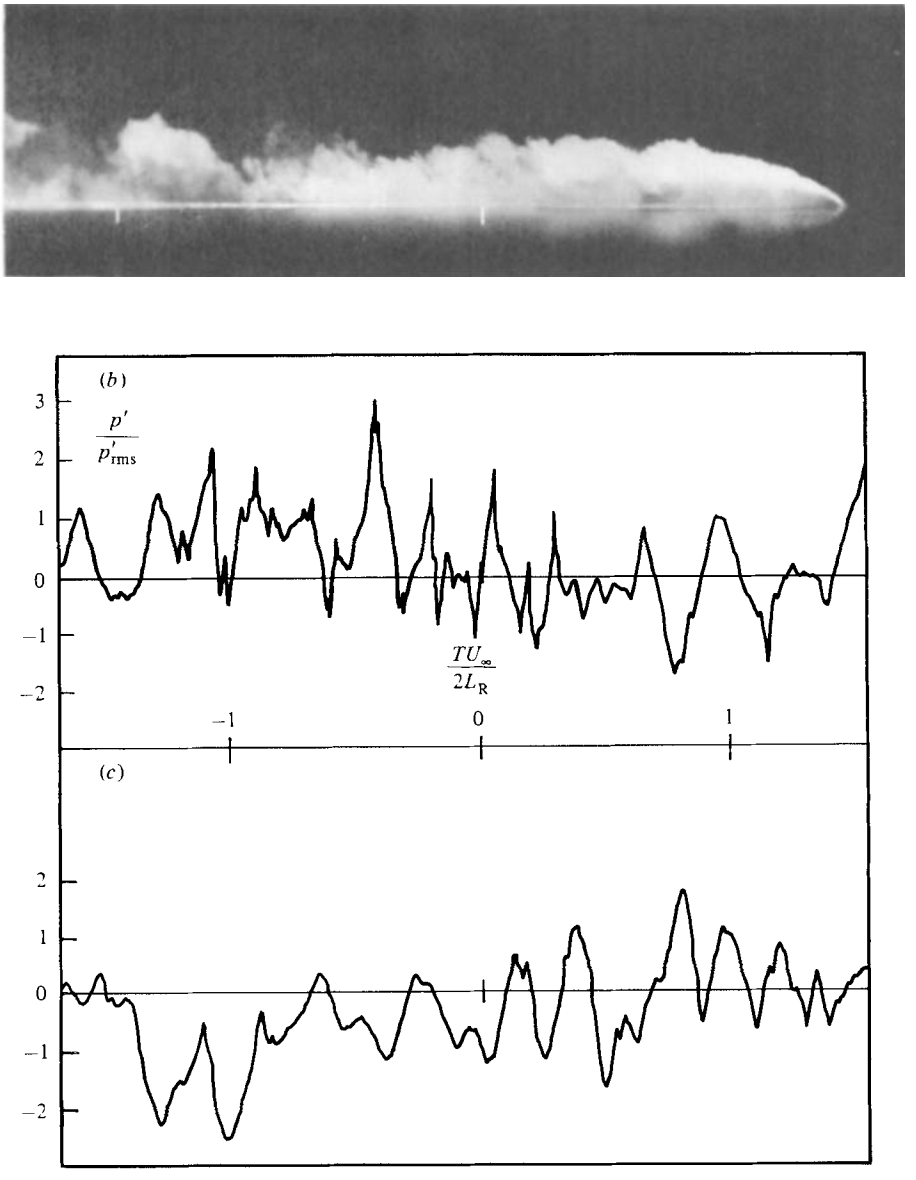

FIGURE 15. Instantaneous smoke flow visualization and simultaneous pressure records. Visualization comments as for figure 12. Pressure trace (*b*) recorded at $X/L_R = 0.97$, $Z = 0$; (*c*) recorded at $X/L_R = 0.27$, $Z = 0$.

fluctuations (or vice versa), which partially reflects a random modulation in the vertical location of the effective centre of vorticity; that is, a strong fluctuation in pressure (say) can indicate either the presence of a strong disturbance or that it happens to have convected close to the surface. This is illustrated well in figure 20(*b*) in fact, where there are two negative pressure excursions of equal magnitude at $TU_\infty/D = 35$ and 54. The second of these coincides with a significant positive-going velocity at the shear-layer edge, whilst the first corresponds to a relatively quiescent velocity phase, so that it originates more probably from a smaller-scale event located closer to the surface. Of course, three-dimensional effects will also be important, so

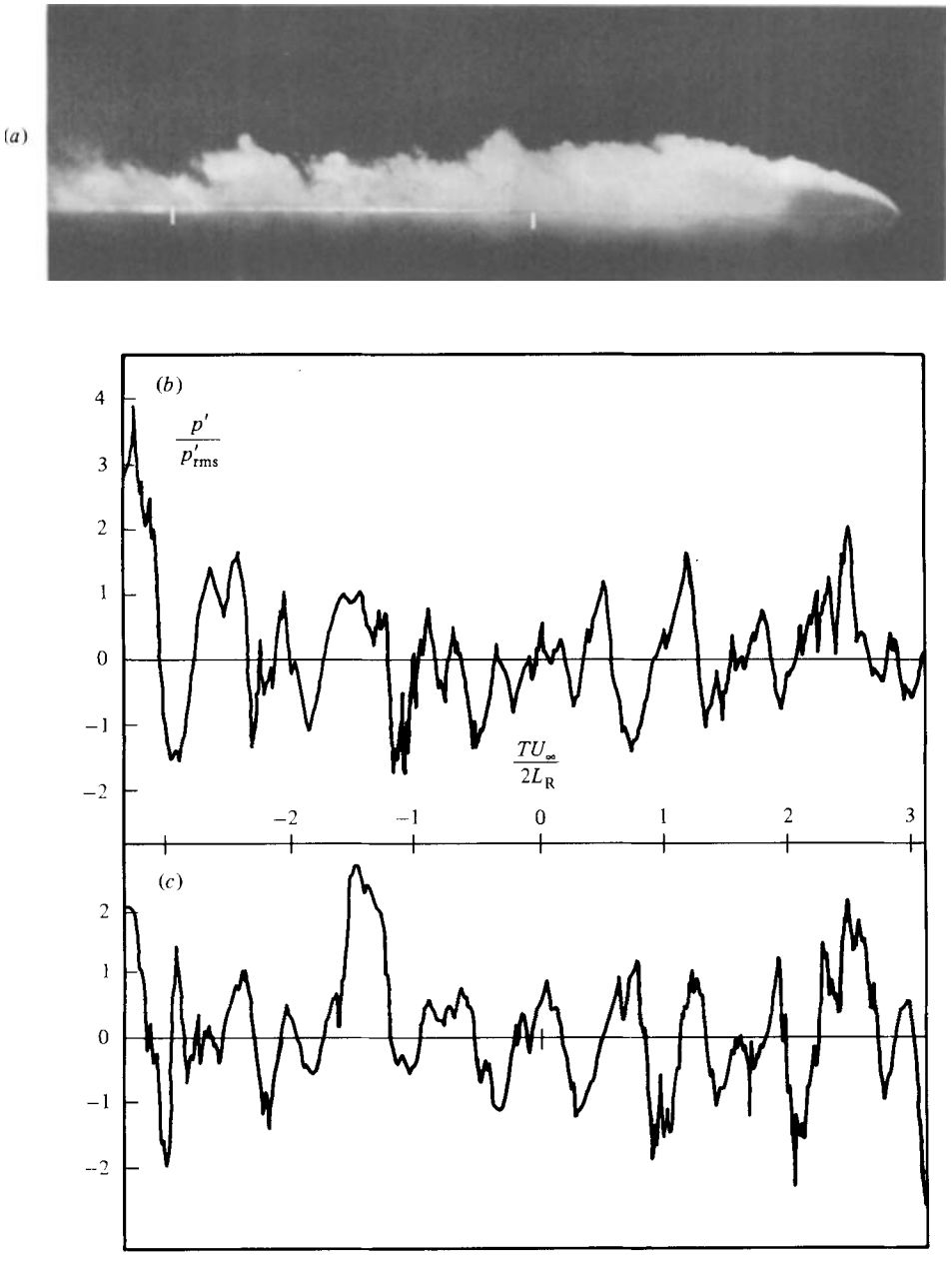

FIGURE 16. Instantaneous smoke flow visualization and simultaneous pressure records. Visualization comments as for figure 12. Pressure trace (*b*) recorded at $X/L_R = 0.97$, $Z = 0$; (*c*) recorded at $X/L_R = 0.97$, $Z/L_R = 0.2$.

that a high correlation cannot always be expected between instantaneous surface-pressure fluctuations and streamwise velocity fluctuations anyway.

Almost certainly the apparent quiescent velocity phase in figure 20 (*b*) corresponds to the typical visualizations shown in figures 15–17, where there is a temporary cessation in the shedding of larger-scale structures from the bubble and an apparent necking of the shear layer downstream. Amongst others, Gartshore & Savill (1982)

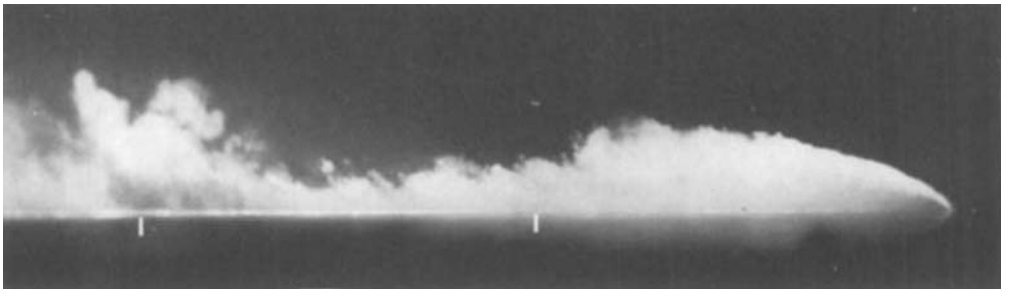

FIGURE 17. Instantaneous smoke flow visualization. Comments as for figure 12.

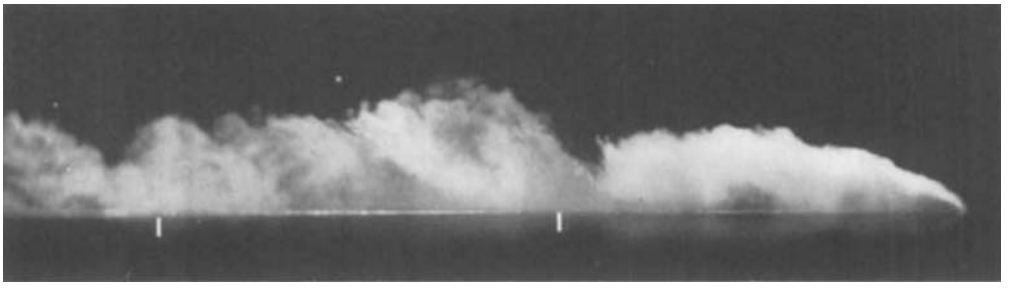

FIGURE 18. Instantaneous smoke flow visualization. Comments as for figure 12.

and H. H. Fernholz (1983 private communication) have also reported a similar necking phenomenon for the flow past a normal flat-plate/splitter-plate configuration. Figure 14 possibly shows the transition from a pseudoperiodic shedding phase to this quiescent phase. Figure 15(*b*) shows the pressure history at $X/L_R = 0.97$, the smaller scale of the structures convecting through the reattachment zone effectively doubling characteristic frequencies compared with the previous records. Again, significant excursions in surface pressure occur, so that extreme fluctuations do not necessarily appear to be associated with any one shedding phase. Superimposed upon this is a low-frequency motion with a period of the same order as, or longer than, the total time of the record (at least 6 in $\Delta T U_\infty / L_R$). This is characteristic time in which a convecting disturbance would travel several bubble lengths, so that it is a plausible timescale for the vorticity shedding to change its character or for the bubble to relax after a large-scale disturbance. The low frequency was detectable throughout the cavity region, often as the amplitude modulation typically shown in figure 14, but it was most apparent in the forward part of the bubble where the difference is the greatest between the low-frequency flapping motion of the shear layer and the small-scale local shear-layer structure. It was not possible to record simultaneous smoke visualizations and pressure traces at tappings very close to separation, but figure 15(*c*) is the pressure history at $X/L_R = 0.27$, matching the visualization of figure 15(*a*) and the reattachment-pressure history of figure 15(*b*). There is a noticeable antiphase relationship between the two low-frequency components, as expected from a bubble lengthening/shortening process ($R_{pp} = -0.15$ from figure 10).

Figures 18 and 19 show vigorous shedding phases, the latter giving the most pronounced shear-layer excursions from over one hundred photographs. Figure 19(*c*) shows corresponding large-amplitude pressure excursions near separation for $T < 0$, at frequencies that would suggest a strong instantaneous correlation between the

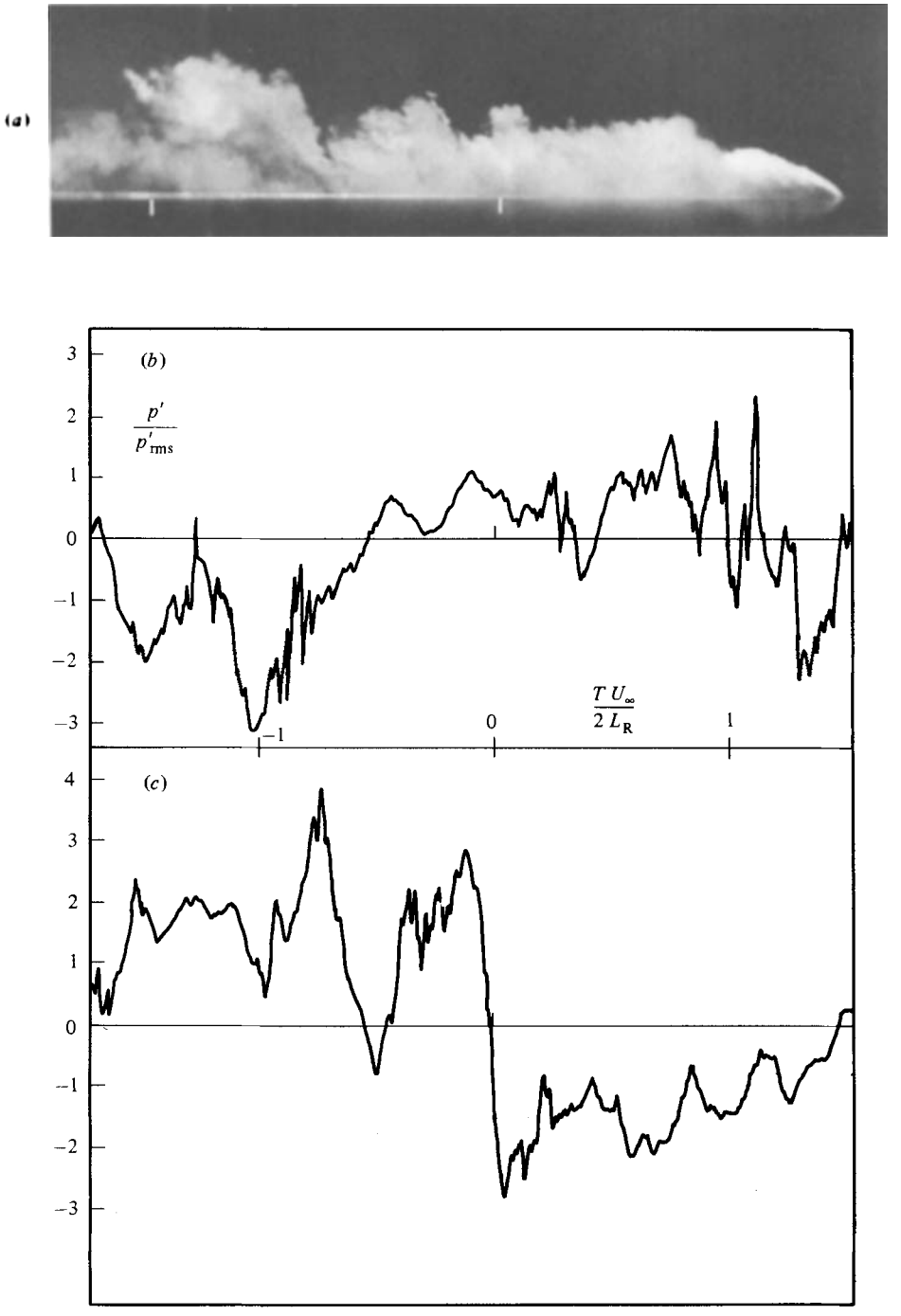

FIGURE 19. Instantaneous smoke flow visualization and simultaneous pressure records. Visualization comments as for figure 12. Pressure trace (*b*) recorded at $X/L_R = 0.97$, $Z = 0$; (*c*) recorded at $X/L_R = 0.27$, $Z = 0$.

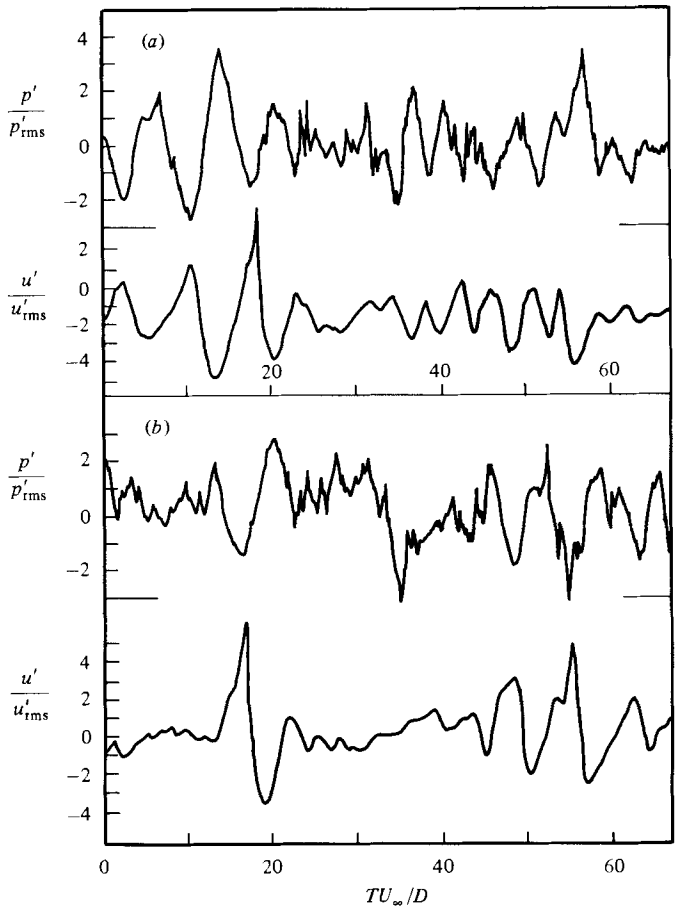

FIGURE 20. Simultaneous pressure and velocity records, with fluctuations normalized by appropriate r.m.s. value. Pressure transducer at $X/L_R = 0.97$. Hot wire at $X/L_R = 0.97$, $Y/L_R = 0.32$ in the essentially irrotational region.

shear-layer roll-up near separation and the vorticity shedding from the bubble, together with an extended relaxation process for $T > 0$. Reattachment-pressure excursions (figure 19*b*) appear to be of no greater magnitude than those shown earlier, so that there is again no strong evidence that large-amplitude reattachment-pressure fluctuations are associated specifically with any one shedding phase.

This last observation on the behaviour of extremes is supported by conditionally sampled pressure measurements made on a similar model in earlier tests (Hillier 1980). In these the surface pressure fluctuations were averaged only when a trigger hot-wire probe located on the model centreline, at $X/L_R = 0.86$ and at a vertical position corresponding to only 5% intermittency, detected a turbulent burst; that is, when there was an extreme shear-layer excursion just before reattachment which presumably indicated that a large-scale structure was about to be shed from the bubble. Figure 21 presents this conditionally averaged pressure p_i (expressed as a departure from the local mean pressure and normalized by the local r.m.s. value) along the model centreline, whilst figure 22 presents more extensive data in the surface (x, z)-plane ($z = 0$ is the centreline). Nowhere do the sampled pressures exceed ± 0.8 r.m.s., so that again the large-scale shear-layer structures do not necessarily

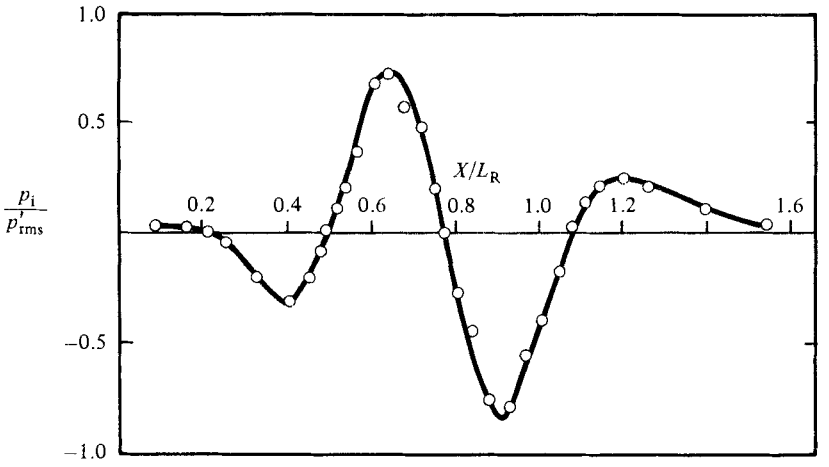

FIGURE 21. Conditionally averaged fluctuating pressure along model centreline taken from Hillier (1980). Trigger hot wire located at $X/L_R = 0.86$, $Z = 0$ at a position of 5% intermittency. Surface pressure sampled only for those periods when the hot wire detects turbulent motion. The conditionally averaged fluctuating pressure is normalized by the local r.m.s. fluctuating pressure.

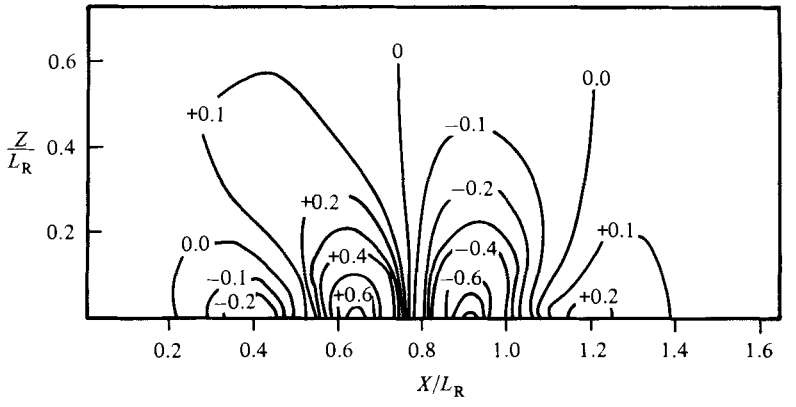

FIGURE 22. Conditionally averaged fluctuating pressure in the (x, z)-plane taken from Hillier (1980). Details as for figure 20.

appear to be, on average, responsible for particularly large-amplitude pressure fluctuations. Some other points should also be noted from these measurements, which are consistent with the correlation measurements to be presented later. First, the conditional pressure decays rapidly with spanwise distance, so that again the shedding of large-scale structures does not appear to be well correlated on average across the span. Secondly, the peak negative pressure occurs close to the trigger-probe position or shear-layer crest, more or less as expected from the earlier visualizations. Thirdly, upstream of the shear-layer crest there is a pronounced positive lobe, indicating on average the position of the shear-layer trough between one structure shedding through reattachment and the next forming near separation (its position presumably marked by the weak negative values of p_i around $X/L_R = 0.4$). In the downstream direction, however, the positive pressure lobe is weak; this asymmetry about the crest seems plausible physically, since the shedding of a large-scale structure from the bubble is likely to influence significantly the roll-up of the

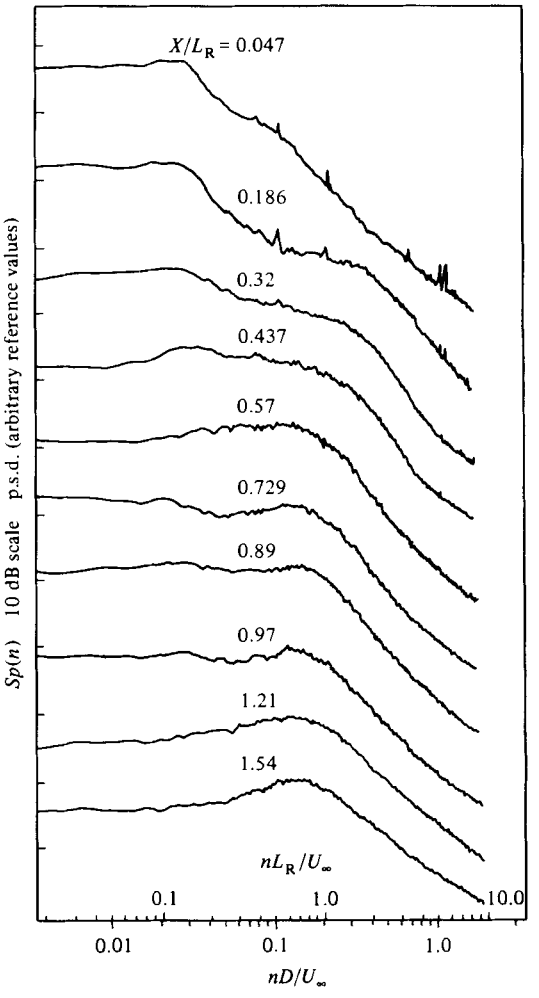

FIGURE 23. Power spectra for surface-pressure fluctuations at various streamwise stations. Arbitrary reference. Scale marked in 10 dB intervals.

subsequent shear-layer disturbance, since it will have shed a significant part of the bubble vorticity, whilst it is not evident that the shedding of a large-scale structure should be well correlated with the immediately preceding event.

7. Pressure spectra

The pressure spectra at various stations along the model centreline are shown in figure 23. These have been corrected for the transducer frequency response characteristics and are cut off above 700 Hz ($nD/U_\infty \approx 2.00$), where the transducer Helmholtz resonance begins. Near separation, where the amplitude of the pressure fluctuations is very low, the spectra are dominated by the low-frequency fluctuations already noted in the previous sections. At $X/L_R = 0.047$, for example, roughly 50% of the energy is at a reduced frequency nD/U_∞ of less than 0.025 (or nL_R/U_∞ less than 0.125), which is about one-fifth of the characteristic frequencies for shedding from the bubble seen in the pressure spectra at reattachment. The absence of energy at high frequencies close to separation can only be attributed in small part to the

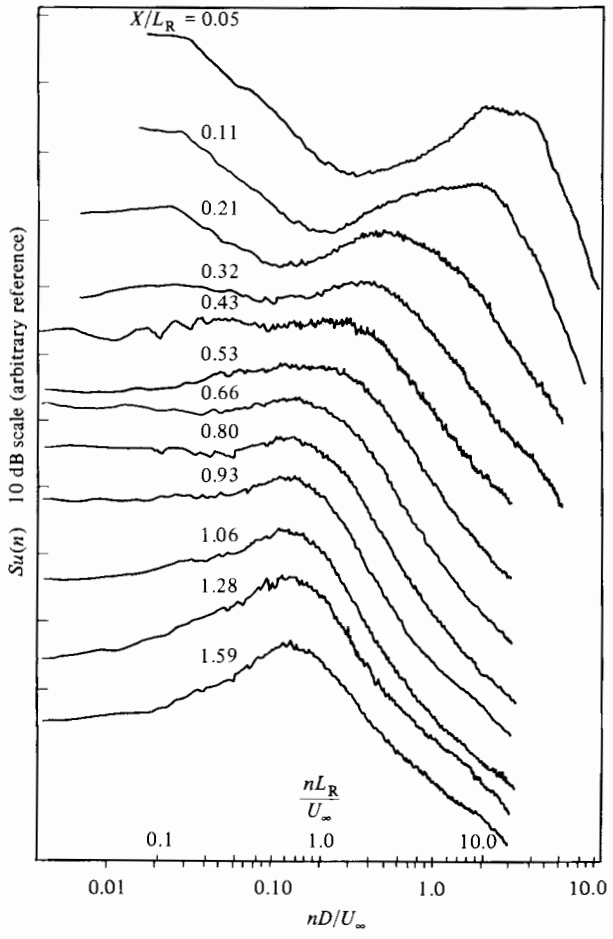

FIGURE 24. Power spectra for velocity fluctuations at various streamwise stations along a locus of 2.5% local intensity. Arbitrary reference. Scale marked in 10 dB intervals.

transducer response characteristics, and mainly shows a spatial filtering effect since the surface is relatively in the far field of the local shear-layer vorticity fluctuations (see figure 24 for spectra of the shear-layer-induced velocity fluctuations measured along the shear-layer edge). The pressure signal is then simply dominated by a residual weak flapping motion of the shear layer (which is also not well correlated across the span, as will become apparent in §9). As remarked earlier, low-frequency fluctuations are evident in other two-dimensional geometries. They are seen in the autocorrelation measurements of fluctuating pressures downstream of a surface-mounted fence (Fricke 1971), in velocity measurements downstream of a rearward-facing step (Eaton & Johnston 1981), and in velocity measurements in the irrotational region just outside the shear layer near separation on the rearward-facing step and the flat-plate/splitter-plate combination (Cherry, Hillier & Latour 1983). Kiya *et al.* (1982) appear also to have noted it in pressure autocorrelation measurements with a geometry similar to the present one. In our present case an effort was made to eliminate the more obvious sources of experimental error which might induce or accentuate the effect. First, unsteady circulation about the model driven (say) by weak stream unsteadiness was not the cause, since a deliberate extension of the chord

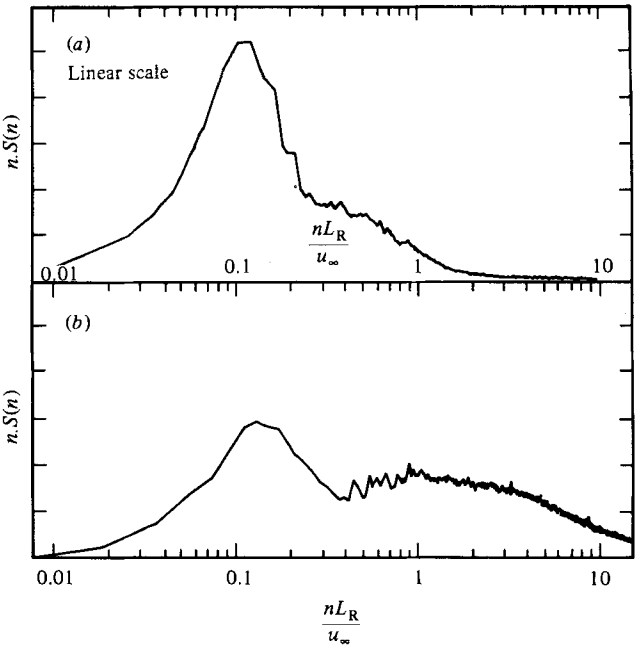

FIGURE 25. Pressure spectra measured at $x/D = 0.125$: (*a*) smooth stream; (*b*) turbulent stream, $u'_{rms}/U_\infty = 9.6\,\%$, $L_X/D = 0.36$.

by 1.22 m produced no change, and because there was zero correlation at all time delays between the foremost pressure tapping and an equivalent one located on the under surface. Secondly, sideplate or aspect-ratio effects can be ignored, because similar low frequencies were found in specific tests made on the axisymmetric equivalent of the model in figure 1. Finally, tunnel acoustics can be discounted, principally because correlation scales are too small (see figure 34), and because the spectral energy is too broad-band and at too low a frequency to correspond to any of the measured acoustic modes. Effects of transition in the shear layer appeared initially to be a possible cause, simply because very-low-Reynolds-number smoke visualizations showed a significant low-frequency variability in the instantaneous transition position. Although this cannot be discounted completely, the balance of evidence is that such effects are weak. In particular transition occurs extremely close to separation anyway at the test Reynolds number, and both the r.m.s. pressure coefficient and dimensionless spectrum at $X/L_R = 0.047$ were unchanged by a doubling of Reynolds number. In addition, the same phenomenon appears anyway in the rearward step separations of both Eaton & Johnston (1981) and also Cherry *et al.* (1983), where separation is already turbulent. The low-wavenumber motion therefore appears to be an integral feature of a fully turbulent separation. This is supported by further measurements made on the model with high levels of grid-generated turbulence in the freestream. Figure 25 compares two spectra at $X/D = 0.125$, one taken from the present smooth-stream study and the other taken with the stream turbulence conditions $(u'_{rms}/U_\infty) = 9.6\,\%$, $L_X/D = 0.36$. For the latter case $C_{p'}$ is 0.115 and the reattachment length has been more than halved to $2.16D$ (see also Hillier & Cherry 1981*b*; Cherry 1982). The turbulent-stream data still show a marked contribution at low frequencies. More significantly, the figure also indicates that this frequency scales best upon the reattachment length, which again identifies the motion as one related to the overall bubble scale.

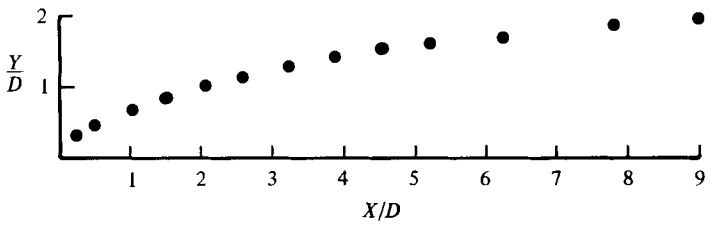

FIGURE 26. Traverse locus for line of 2.5% local intensity. Measurements of velocity spectra and spanwise velocity correlations were made along this line.

Progressing further downstream from separation, the combined effect of the growth of shear-layer scales and the progressive turning of the shear layer towards the surface produces an increasing near-field contribution to the surface pressure fluctuations, shown by the increase of $C_{p'}$ in figure 9 and by the emergence of a higher-frequency contribution in the spectra of figure 23. With increasing distance from separation, this latter contribution reduces in frequency as expected, but by about 60% of the bubble length the spectra become dominated by a broad-band shedding of vorticity from the bubble. Subsequent spectral changes are only slow, even though the earlier velocity-profile measurements show that the shear-layer thickness increases right up to reattachment.

8. The velocity spectra

Figure 24 shows velocity spectra for a traverse along a locus of 2.5% local intensity at the shear-layer edge; this locus is shown in figure 26. The velocity fluctuations here are essentially irrotational, with turbulent bursts noted only rarely. Indeed, of the many instantaneous smoke visualizations taken, only figure 19 shows a definite shear-layer excursion outside this locus. No intermittency measurements have been made, but Wygnanski & Fiedler (1970) give a value of about 0.5% at an equivalent position in the plane mixing layer. These irrotational velocity spectra and the surface-pressure spectra presented earlier are both driven by the same shear-layer vorticity fluctuations and large-scale bubble motions. There are differences, however, because the locations of the pressure transducers and hot wires relative to the source region are not equivalent. Thus near separation the spatial filtering effect means that the low-frequency flapping motion dominates the surface-pressure spectra, but for the hot wire that is placed much closer to the shear layer, virtually all of the velocity fluctuation energy is now at much higher frequencies. Nonetheless, the two main features shown by the velocity spectra underline those found by analysis of the pressure spectra, namely the initial progressive fall in frequency with streamwise distance of the fluctuations driven by the local shear-layer structure, and then the appearance of a shedding contribution which dominates the approach to reattachment and the development downstream. A simple measure of this frequency variation is shown in figure 27, where the frequencies are taken directly from the appropriate spectral peaks of figure 24. In the central region of the bubble there is an overlap between the two processes, but it should be noted that there is no abrupt change in spectral characteristics in this region, however, simply the progressive dominance of one process over the other. This is shown better in figure 28 by the chordwise variation of the frequency $n_{0.5}$ that divides the velocity spectrum into two halves of equal energy. This varies smoothly from separation up to reattachment. Normalized by the characteristic separation velocity $U_s = U_\infty(1-C_{ps})^{0.5}$, where C_{ps} is evaluated at the

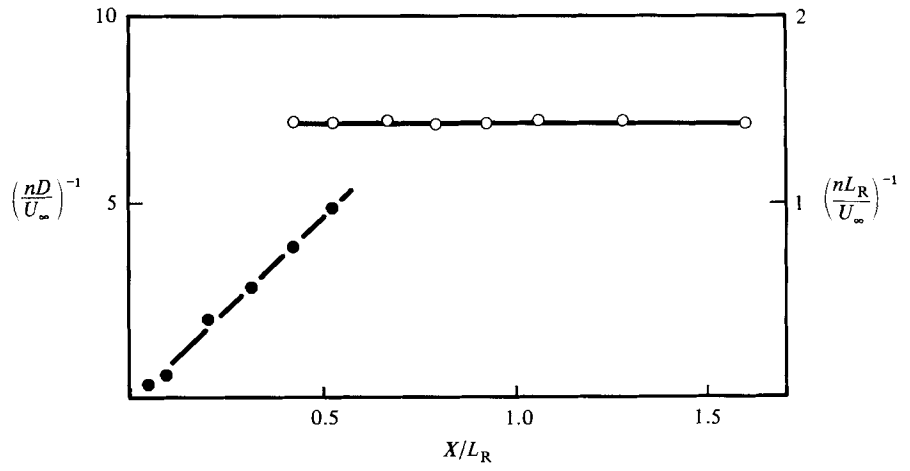

FIGURE 27. Frequency variation with distance of significant peaks from the velocity spectra of figure 24: ●, detection of frequencies corresponding to the local large-scale structure of the shear layer; ○, detection of a characteristic shedding frequency.

pressure tapping closest to separation, the data agree well with irrotational velocity measurements made by McGuinness (1978) on an internal separated flow in the entry region of a pipe which are shown in the same figure.

The dominant frequency for shedding from the bubble, obtained from the velocity spectra, corresponds to a value of nL_R/U_∞ of about 0.7, which agrees well with the values of McGuinness (1978) and the range found by Mabey (1971) for a variety of two-dimensional separated and reattaching flows. Cherry *et al.* (1982) have also shown similar values for the rearward step separation and the separation formed by a normal flat-plate/splitter-plate combination. Figure 29 compares these last two configurations with the present data.

9. Space–time correlations

9.1. *Spanwise correlations R_{uu} and R_{pp}*

There are very few measurements of spanwise correlations in separated and reattaching flows, despite the obvious importance of unsteady three-dimensional effects both in the initial shear-layer development immediately downstream of separation and transition, and also in the dynamics of the reattachment process, which might be expected to accentuate any three-dimensional irregularities in the spanwise vortex structure. In the present experiments spanwise correlations of streamwise velocity fluctuations were made at the shear-layer edge (at the same locus of 2.5% local intensity as in the spectral measurements of figure 24) together with spanwise correlations of the fluctuating surface pressure at various streamwise stations.

The velocity correlations of figure 30 show a progressive increase of spanwise scale with distance, and figure 31 gives a measure of this growth where both the lateral integral scale λ_Z and the hot-wire spacing $\Delta Z_{0.4}$ for a 40% correlation coefficient are shown. The lateral integral scale λ_Z is evaluated from the area under the appropriate correlation curve of figure 30, and is actually a slight underestimate since R_{uu} does not fall to zero for the maximum wire separation used. This figure reveals a surprisingly linear increase of lateral correlation length almost up to the time-

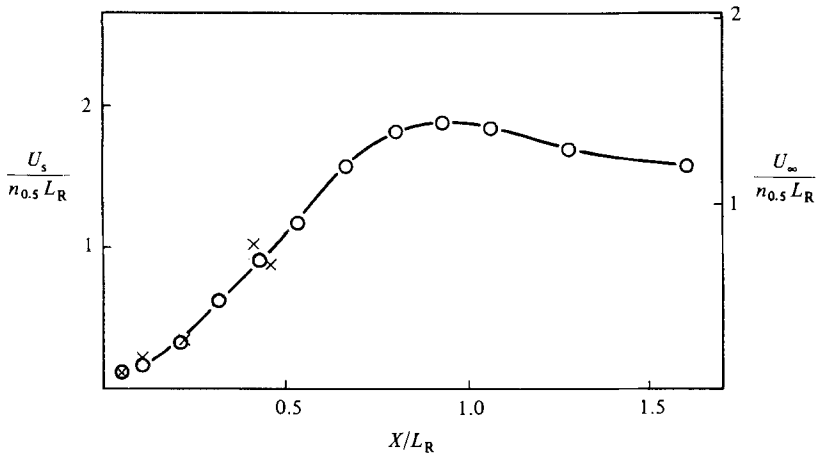

FIGURE 28. Variation with distance of the frequency dividing the velocity spectra of figure 24 into two halves of equal energy, (○), and internal separated flow at pipe entry (McGuiness 1979), (×).

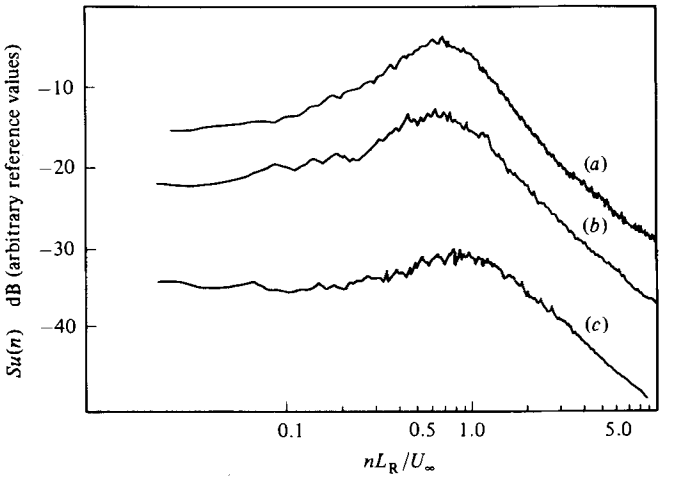

FIGURE 29. Velocity spectra in irrotational flow outside the shear layer at reattachment: (*a*) present tests. Cherry *et al.* (1982): (*b*) normal flat-plate/splitter-plate combination; (*c*) rearward-step/splitter-plate combination.

averaged reattachment position, beyond which only a much reduced growth remains. However, figure 32, which plots R_{uu} against Z/λ_Z, shows that there is not a completely self-similar development up to reattachment.

Smoke flow visualization from above the model at very low Reynolds number showed that initially vortex filaments were shed parallel to the separation edge with an obvious spanwise coherence extending many local shear-layer thicknesses, but that the onset of transition was marked by the rapid development of three-dimensionality and helical pairing, similar to that visualized by Clark & Kit (1980) and by Gartshore & Savill (1982). Presumably a similar development would take place at the test Reynolds number, but confined to a much shorter streamwise distance, so that approaching sufficiently close to separation the trend of decreasing lateral correlation shown in figure 31 can be expected to reverse. However, difficulties

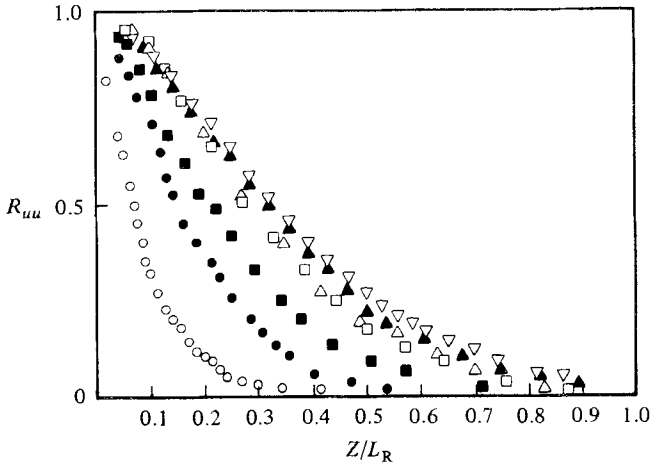

FIGURE 30. Spanwise cross-correlation coefficient R_{uu} for streamwise velocity fluctuations taken along locus of 2.5% local intensity: ○, $X/L_R = 0.26$; ●, 0.53; ■, 0.71; □, 0.89; △, 1.0; ▲, 1.18; ▽, 1.40.

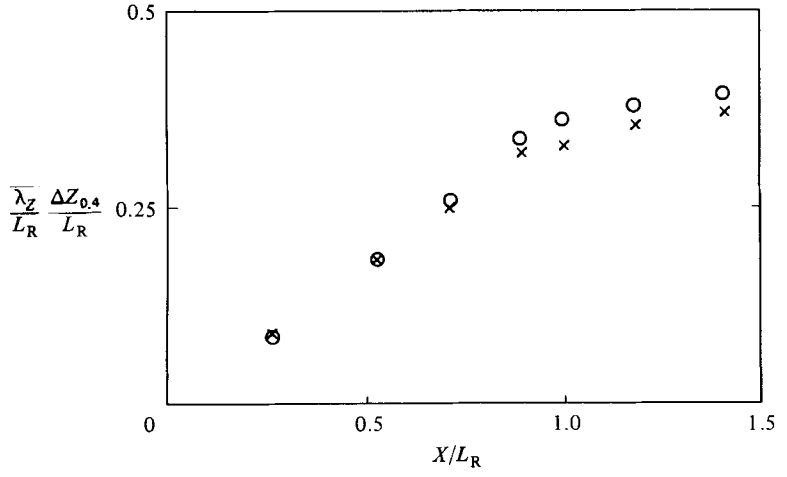

FIGURE 31. Variation with distance of lateral integral scale λ_Z (×), and hot wire separation $\Delta Z_{0.4}$ for a 40% correlation coefficient (○).

in obtaining adequate spatial resolution meant that measurements in this region were not worthwhile. It seems unlikely that serious effects of transition persist for any significant streamwise distance from separation, since it was found that within measurement accuracy (better than ± 0.02 in R_{uu}) the correlations were unchanged by a doubling of Reynolds number. This suggests that very rapidly after separation the shear layer approaches some asymptotic three-dimensional state. There also appears to be no strong specific three-dimensionalizing effect of reattachment upon the larger shear-layer scales, since the virtual cessation in growth of the lateral correlation scale downstream of reattachment is consistent with the much reduced growth in shear-layer thickness. At reattachment the vorticity thickness δ_w of the shear layer ($\delta_w = U_{max}/(dU/dy)_{max}$) is approximately $0.87D$ or $0.178L_R$, so that λ_Z is $1.83\delta_w$ and $\Delta Z_{0.4}$ is $1.97\delta_w$. These data are similar to those found for plane mixing layers: Browand & Troutt (1980) measured correlations on the low-velocity side of a mixing layer (with 8:1 velocity ratio), quoting an asymptotic value (i.e. sufficiently

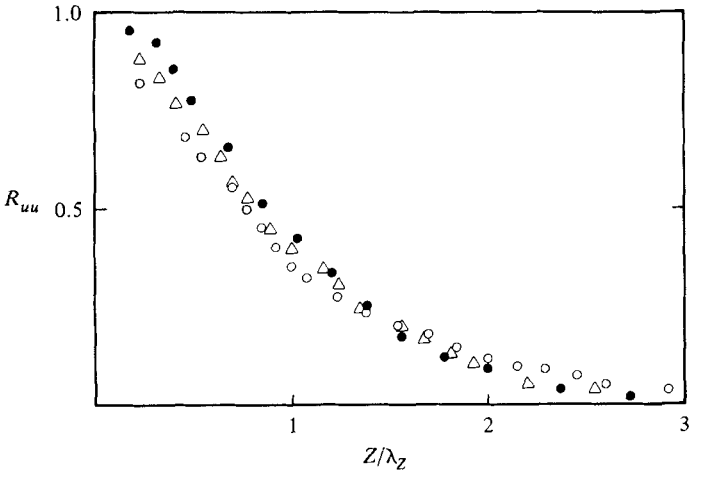

FIGURE 32. Spanwise correlation with hot wire separation Z normalized by λ_Z: ○, $X/L_R = 0.26$; △, 0.53; ●, 0.89.

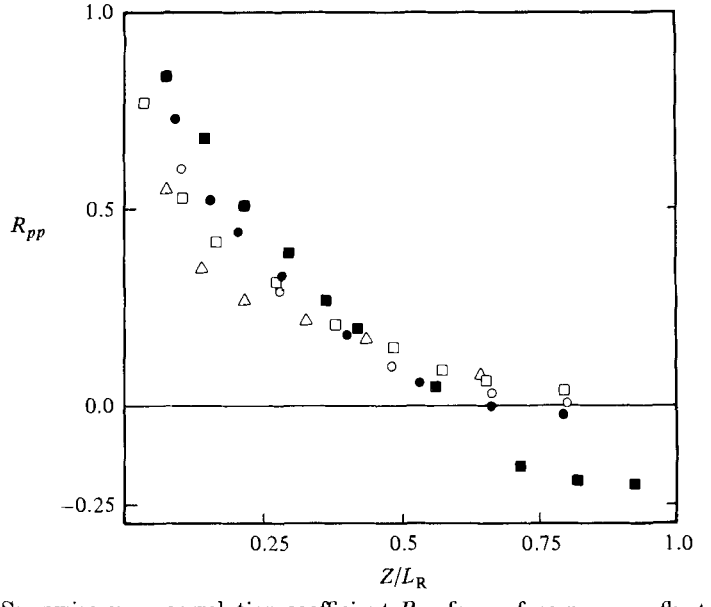

FIGURE 33. Spanwise cross-correlation coefficient R_{pp} for surface-pressure fluctuations: ■, $X/L_R = 0.05$; ●, 0.27; ○, 0.64; □, 0.97; △, 1.54.

far from the origin for transitional effects to have disappeared) of $2.3\delta_w \pm 0.25\delta_w$ for $\Delta Z_{0.4}$, at a location corresponding to 2% irrotational velocity fluctuations.

The spanwise surface-pressure cross-correlations of figure 33 contrast distinctly with those for the velocity, in particular very close to separation where pressure fluctuations are dominated by the low-frequency flapping motion. Here R_{pp} falls to zero for a transducer spacing of about $0.6L_R$, followed by a weak negative lobe. This was not the result of any mean phase-angle change or time lag between the two transducers themselves, so that there is a weak tendency for out-of-phase shear-layer flapping motions to develop over spanwise separations of $0.6L_R$ or so. This probably

indicates that some unsteady lateral venting of fluid within the cavity region is part of the low-frequency process – perhaps the simultaneous appearance across the span of cells with different shedding characteristics (possibly the large-scale shedding and small-scale shedding remarked upon earlier). Further downstream the correlations show a more rapid fall for small transducer separations, accompanied by the disappearance of the negative lobe, so that the pressure source appears to become progressively more three-dimensional. This differs from the behaviour of the velocity correlations, but serves to show that a significant part of the pressure fluctuations in the reattachment region derive from smaller-scale turbulent motions deeper within the shear layer, which are not detected very effectively by velocity measurements restricted to the irrotational zone.

For a few of the smoke flow visualizations simultaneous pressure records were taken with two transducers at reattachment, one on the centreline and one with a small spanwise separation of $1D$ (about $0.2L_R$), which gives a time-average correlation coefficient of about 0.37 between the two. Such a visualization is shown in figure 13, where shedding is by a sequence of more-or-less discrete structures; there is a clear instantaneous correlation between the two stations, and the major fluctuations at each can be matched without difficulty. In figure 16 signals at the same positions are presented for a longer time record, which corresponds roughly to the time required for a disturbance to convert some $6L_R$. Thus the shear-layer disturbances visible in the smoke flow in the region $1 < X/L_R < 2$ all passed through reattachment in the approximate interval $-1 < TU_\infty/2L_R < 0$, which is characterized in figure 16(*b*) by fairly high-frequency motions compatible with the smaller scale of shedding structure seen. Off the centreline, however, figure 16(*c*) shows that this interval is characterized by structures shedding at about half the frequency, so that possibly this shows a spanwise coalescence mechanism. Outside this time interval both traces show more extended shedding at lower frequency. It is possible to find intervals when the signals are in phase (e.g. $TU_\infty/2L_R = -1.5$) and out of phase ($TU_\infty/2L_R = 0.75$), so that, instantaneously, it appears that strong streamwise inclinations of the pressure-generating structures can occur. It remains to be seen from further instantaneous measurements with multisensor arrays of hot-wire probes, whether instantaneously there is evidence of extended spanwise structures with spanwise coalescences or bifurcations, and the generation of local trailing vorticity components. Such phenomena have been noted for mixing layers by Browand & Troutt (1980).

9.2. *Pressure–velocity correlations*

Measurements of pressure–velocity correlations have been restricted to only a few pressure tapping positions, principally at separation and reattachment, with the hot wire mainly located in the irrotational or low-intensity regions. Figures 34 and 35 show the correlations between a hot-wire traversing the (X, Y)-plane on the model centreline and pressure transducers located respectively near separation (at $X/L_R = 0.027$) and near reattachment ($X/L_R = 0.97$). In figure 34 the pressure fluctuations are dominated by the low-frequency flapping motion, so that there is a strong negative correlation between the tapping and the hot wire located in the external irrotational flow. Vertically the correlation falls fairly rapidly, largely reflecting the limited spatial coherence of the flapping motion already observed in the spanwise correlations. Further downstream a region of positive correlation forms between separation and reattachment, which is in the sense expected from a quasi-steady bubble-shortening–lengthening process.

In figure 35 the correlation forms extreme negative values ($R_{pu_{\min}} \approx -0.65$) almost

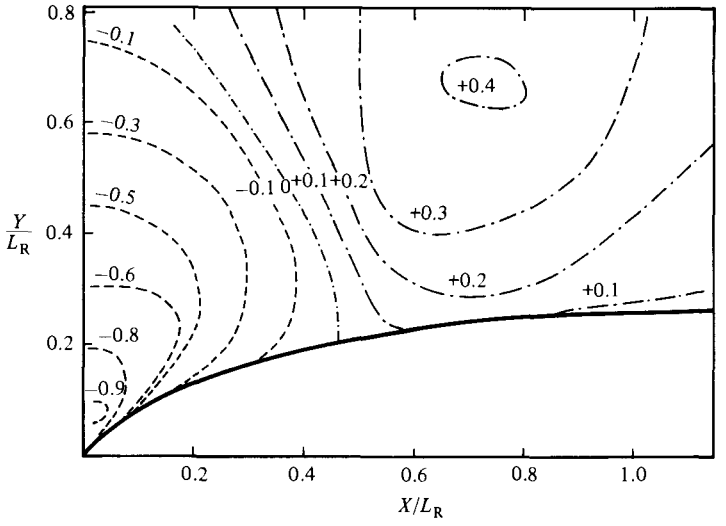

FIGURE 34. Cross-correlation R_{pu} at zero time delay between the fluctuating pressure at $X/D = 0.125$ ($X/L_R = 0.027$) and irrotational velocity fluctuations outside the shear layer. —— marks the approximate position of the shear-layer edge (contour of 2.5% local turbulence intensity).

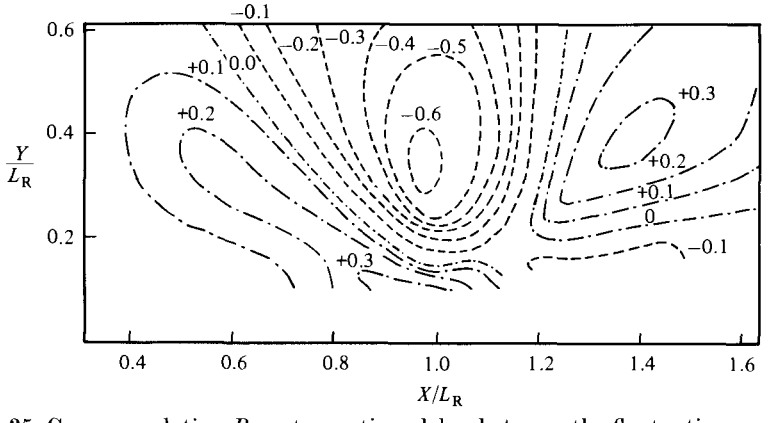

FIGURE 35. Cross-correlation R_{pu} at zero time delay between the fluctuating pressure at $X/D = 4.75$ ($X/L_R = 0.97$) and the streamwise velocity fluctuations.

directly above the tapping, with pronounced regions of positive correlation both upstream and downstream. This correlation is the pattern expected from a vortex-like source, the inclination of the positive lobes upstream and downstream generally reflecting the effect expected from the combined influence of a vortex source and its image reflection in the surface. Penetrating closer to the surface so that the shear layer is entered, the correlation changes sign, again as expected.

This change of sign is illustrated more clearly by figure 36, where R_{pu} is plotted specifically for a traverse vertically above the tapping. The figure also includes correlation measurements at the same station on nominally the same geometry made by Kiya *et al.* (1982), showing close agreement between the two experiments. Entering the shear layer from the external irrotational flow, R_{pu} reaches a minimum at roughly the same position as where the first turbulent bursts were detectable (about 2.5% local intensity), and the subsequent variation in magnitude is determined mainly by

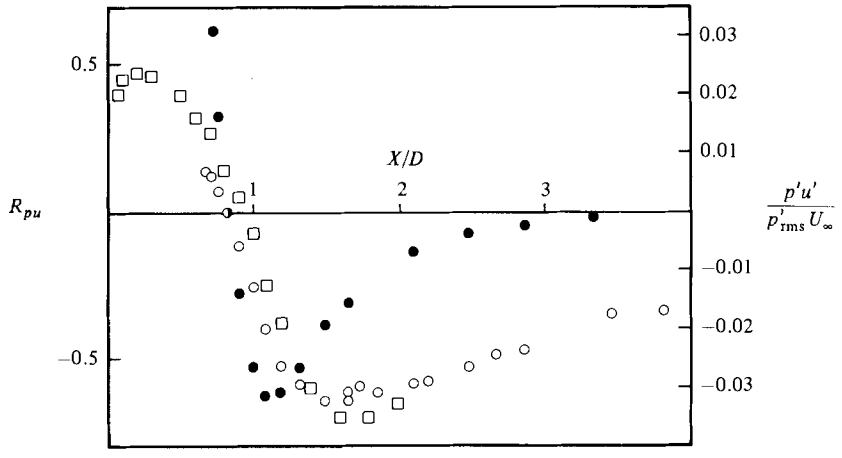

FIGURE 36. Variation of pressure–velocity correlation directly above pressure tapping at $X/L_R = 0.97$: ○, R_{pu} from present work; □, R_{pu} from Kiya *et al.* (1982) for $X/L_R = 1.04$; ●, $\overline{p'u'}$ from present work.

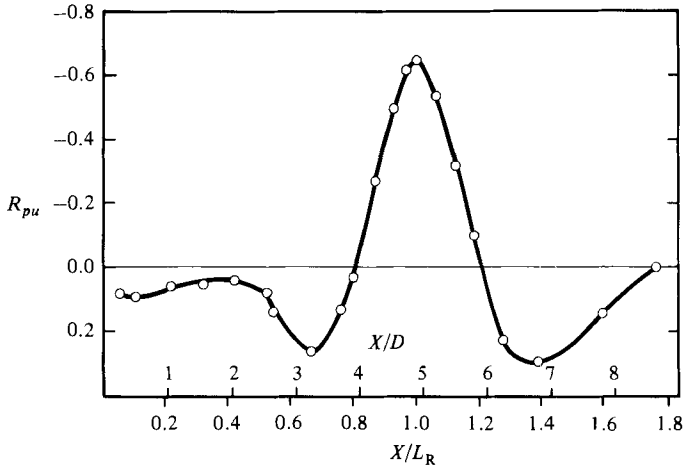

FIGURE 37. Cross-correlation between surface pressure fluctuations at $X/L_R = 0.97$ and streamwise velocity fluctuations taken along 2.5% local intensity contour.

the rapid increase of turbulence intensity at the smaller scales, which are less effective as pressure sources. Consideration of the term $\overline{p'u'}$ alone is perhaps more useful, therefore, and this is also shown in figure 36, where the minimum now occurs well within the intermittent region ($Y/D \approx 1.5$; $u'_{rms}/U \approx 6\%$). The location of zero correlation ($Y/D \approx 1.15$, $u'_{rms}/U \approx 19\%$) must lie at a mean position close to the average centre of vorticity of structures convecting through reattachment, and the distance from this zero to the extreme negative value of $\overline{p'u'}$ provides some measure of the vortex-core radius and the random modulation in vertical position of the effective vortex centres, which was remarked upon earlier in §6.

Figure 37 presents the correlation at zero time delay between a pressure tapping located at $X/L_R = 0.97$ and a hot wire traversed along 2.5% intensity contour, whilst figure 38 shows corresponding time-lagged correlations. In figure 38 the development of the correlation with spacing between the hot wire and the transducer is very similar

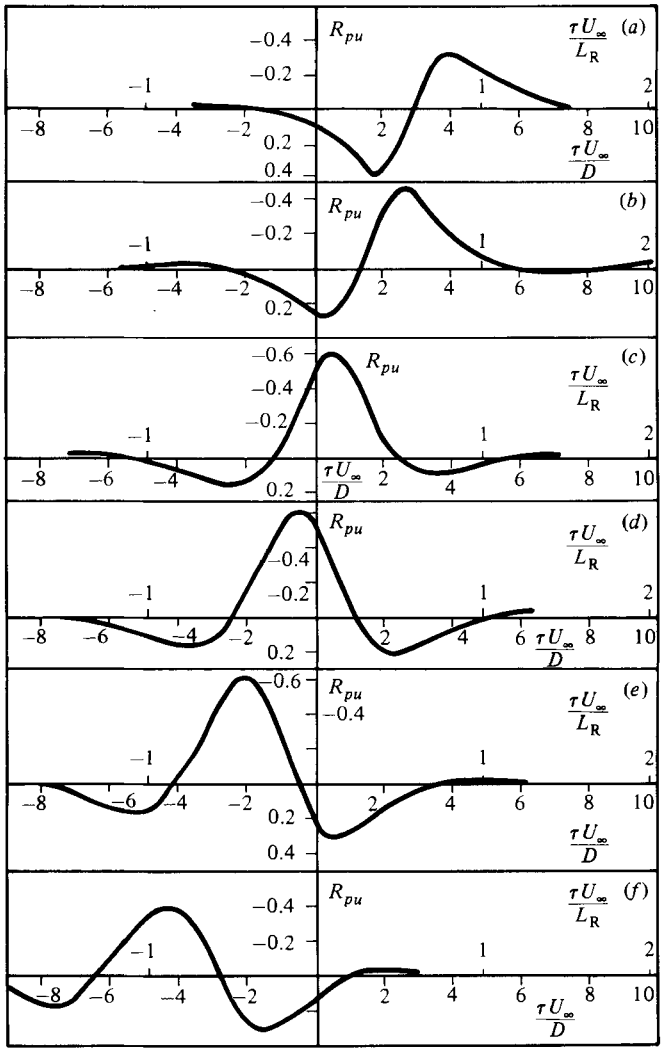

FIGURE 38. Time-lagged cross-correlation between pressure fluctuations at $X/L_R = 0.97$ and hot wire at various streamwise locations of 2.5% local intensity. Time delay τ is positive for velocity delayed with respect to pressure: (*a*) $X/L_R = 0.53$; (*b*) 0.67; (*c*) 0.97; (*d*) 1.06; (*e*) 1.28; (*f*) 1.59.

to that shown in figure 11 for surface-pressure cross-correlations (except of course that the signs of the correlations are different) – in particular, the clear convection of disturbances in the freestream direction and the eventual dominance of a weak low-frequency motion for large spacings. Figure 39 provides a measure of convection speed by plotting τ_{max}, the time delay to peak positive or negative correlation for R_{pp} and R_{pu} respectively, against separation. In the reattachment region the slope of this curve gives a measure of convection speeds, approximately 50% U_∞ from the pressure–pressure cross-correlations and 63% U_∞ from the pressure–velocity measurements. The somewhat higher value of the latter probably reflects that a correlation taken across the shear layer is biased more towards the larger-scale sources and hence the higher convection speeds.

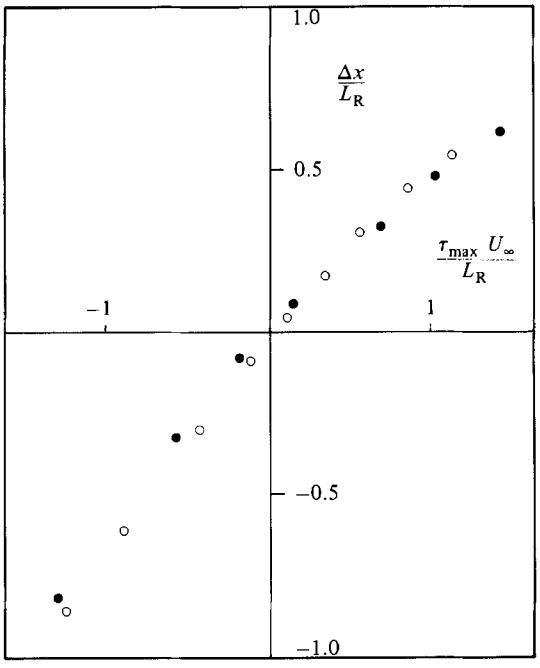

FIGURE 39. Variation with separation of time delay τ_{max} for maximum correlation R_{pp} and minimum correlation R_{pu}. Pressure transducer at reattachment. Positive Δx for hot wire or moveable transducer upstream of fixed transducer. ●, pressure–velocity correlation; ○, pressure–pressure correlation.

10. Discussion and concluding remarks

The shear-layer development, and hence the development of the surface-pressure fluctuations, appears to divide into three distinct but interrelated effects. Near separation a low-frequency flapping motion is dominant in the surface-pressure fluctuations, principally because the surface is in the far field of the local shear-layer fluctuations. We associate this frequency, which is also found in other studies, with the characteristic timescale for the relaxation from one particular shedding phase to another, which probably reflects some overall bubble growth–decay mechanism. Spanwise correlation scales are small, however, so that, instantaneously, various different shedding phases will occur across the span even for quite low-aspect-ratio experiments. From transition up to some 60 % of the bubble length, the mixing layer can grow in relative isolation from the effects of the reattachment surface, and the nearly linear growth of characteristic frequencies, shear-layer thickness and lateral correlation scales are all similar to values found for the fully developed plane mixing layer and other separated-flow experiments. Departures from self-similar development in the separated flow then appear to be associated with the presence of the reattachment surface, shear-layer curvature, etc., rather than with the relatively low Reynolds number of the tests. At reattachment and downstream, the shear-layer growth appears to cease fairly abruptly. Shedding of vorticity from the bubble varies through a range of phases, including a large-scale motion with occasional pseudoperiodic bursts to shedding of small-scale structures which appears to indicate a temporary interruption to the shear-layer-structure growth/coalescence process. Pseudoperiodic shedding has been observed in other configurations (Welsh & Gibson

1979; Parker & Welsh 1982), where it has been indicated that the effect can be amplified or stimulated by acoustics. During the present work there was never any evidence of interaction between the very low level of acoustics and the flow field.

Lateral correlations are less than the bubble length, and for the shear-layer velocity fluctuations they agree quite well with plane mixing-layer data. Perhaps surprisingly there is no significant reduction in spanwise correlation scale (for the irrotational fluctuations) downstream of reattachment, so that at least for the larger shear-layer scales there is no apparent (strong) three-dimensionalizing effect of reattachment. This is somewhat contrary to suggestions made by Kiya *et al.* (1982) amongst others, who suggested that the failure of their discrete-vortex model to predict Reynolds stresses adequately near reattachment really reflected the strong appearance of three-dimensional effects there. The implication from the spanwise velocity correlations is that instead a three-dimensional state is achieved well before reattachment and that this is not particularly accentuated by the reattachment process itself. Pressure cross-correlations, on the other hand, do show a progressive fall of lateral scales with distance, although the reasons for this are more difficult to interpret since the relative source position within the shear layer changes also with streamwise distance. In particular, the pressure correlations downstream of reattachment do show a continued fall in correlation for small transducer spacings, which perhaps indicates a three-dimensionalizing of the smaller scales. Perhaps this would also be shown by velocity correlations if measurements were made deeper in the shear layer and this is intended to be the subject of further work.

N. J. Cherry was in receipt of a Case Studentship from the S.E.R.C. The work was supported in part by the Building Research Establishment.

REFERENCES

ARIE, M. & ROUSE, H. 1956 Experiments on two-dimensional flow over a normal wall. *J. Fluid Mech.* **1**, 129–142.

ASHURST, W. T. 1979 Calculation of plane sudden expansion via vortex dynamics. *Sandia Lab. Rep.* SAND 79–8679.

BREDERODE, V. A. S. L. DE 1975 Three dimensional effects in nominally two-dimensional flows. Ph.D. thesis University of London.

BROWAND, F. K. & TROUTT, T. R. 1980 A note on spanwise structure in the two-dimensional mixing layer. *J. Fluid Mech.* **97**, 771–781.

BROWN, G. L. & ROSHKO, A. 1974 On density effects and large structure in turbulent mixing layers. *J. Fluid Mech.* **64**, 775–816.

CASTRO, I. P. & DIANAT, M. 1983 Surface flow patterns on rectangular bodies in thick boundary layers. *J. Wind Engng Indust. Aero.* **11**, 107–119.

CHANDRSUDA, C. 1976 A reattaching turbulent shear layer in incompressible flow. Ph.D. thesis, University of London.

CHERRY, N. J. 1982 The effects of stream turbulence on a separated flow with reattachment. Ph.D. thesis, University of London.

CHERRY, N. J., HILLIER, R. & LATOUR, M. E. M. P. 1983 The unsteady structure of two-dimensional separated and reattaching flows. *J. Wind Engng Indust. Aero.* **11**, 95–105.

CHEUNG, W. S. 1982 Heat transfer in low speed separated flows. Ph.D. thesis, University of London.

CLARK, J. A. & KIT, L. 1980 Shear layer transition and the sharp edged orifice. *Trans. ASME I: J. Fluids Engng* **102**, 219–225.

EATON, J. K. & JOHNSTON, J. P. 1981 A review of subsonic turbulent flow reattachment. *AIAA J.* **19**, 1093–1100.

ETHERIDGE, D. W. & KEMP, P. H. 1978 Measurements of turbulent flow downstream of a rearward-facing step. *J. Fluid Mech.* **86**, 545–566.

FRICKE, F. R. 1971 Pressure fluctuations in separated flow. *J. Sound Vib.* **17**, 113–123.

GARTSHORE, I. P. & SAVILL, M. 1982 Some effects of free stream turbulence on the flow around bluff bodies. Euromech 160: Periodic Flow and Wake Phenomena, Berlin.

HILLIER, R. 1980 Measurements of mean and fluctuating pressures in a separated flow. *IC Aero. TN* 80–108.

HILLIER, R. & CHERRY, N. J. 1981*a* Pressure fluctuations under a turbulent shear layer. In *Proc. 3rd Symp. on Turbulent Shear Flows, Univ. California, Davis*, pp. 23–29.

HILLIER, R. & CHERRY, N. J. 1981*b* The effects of stream turbulence on separation bubbles. *J. Wind Engng and Indust. Aero.* **8**, 49–58.

KATSURA, J. 1976 Fluctuating wind pressure on the side surfaces of models with long rectangular sections. In *Proc. 2nd USA–Japan Res. Seminar on Wind Effects on Structures* (ed. H. Ishizaki & A. N. L. Chiu), pp. 113–124. University of Tokyo Press.

KIYA, M., SASAKI, K. & ARIE, M. 1982 Discrete vortex simulation of a turbulent separation bubble. *J. Fluid Mech.* **120**, 219–244.

LATOUR, M. E. M. P. & HILLIER, R. 1980 Experiments on a two-dimensional separated flow. *IC Aero. TN* 80–101.

MABEY, D. G. 1971 Pressure fluctuations caused by separated bubble flows at subsonic speeds. *RAE Tech. Rep.* 71160 ref. Aero 3204, August 1971.

MCGUINNESS, M. D. 1978 Flow with a separation bubble: steady and unsteady aspects. Ph.D. thesis, University of Cambridge.

MOSS, W. D. & BAKER, S. 1980 Recirculating flows associated with two-dimensional steps. *Aero Q.* **31**, 151–172.

OTA, T. & ITASKA, M. 1976 A separated and reattached flow on a blunt flat plate. *Trans. ASME* I: *J. Fluids Engng* **98**, 79–86.

PARKER, R. & WELSH, M. C. 1982 The effect of sound on flow over bluff bodies. In *Proc. 3rd Keswick Intl Conf. on Vibration in Nuclear Plant, Keswick, England.* Brit. Nucl. Energy Soc., London.

ROSHKO, A. & LAU, J. 1965 Some observations on transition and reattachment in a free shear layer in incompressible flow. *Proc. Heat Transfer Fluid. Mech. Inst. 18* (ed. A. F. Charwat), pp. 157–167. Stanford University Press.

WELSH, M. C. & GIBSON, D. C. 1979 Interaction of induced sound with flow past a square leading edged plate in a duct. *J. Sound Vib.* **67**, 501–511.

WESTPHAL, R. V., EATON, J. K. & JOHNSTON, J. P. 1981 A new probe for measurement of velocity and wall shear stress in unsteady reversing flow. *Trans. ASME* I: *J. Fluids Engng* **103**, 478–483.

WYGNANSKI, I. J. & FIEDLER, H. E. 1970 The two-dimensional mixing region. *J. Fluid Mech.* **41**, 327–361.